

## Article

# Numerical Study of Smoke Distribution in Inclined Tunnel Fire Ventilation Modes Considering Traffic Conditions

Po-Wei Tung <sup>1,2</sup>, Hung-Chieh Chung <sup>1,3,\*</sup>, Nobuyoshi Kawabata <sup>4</sup>, Miho Seike <sup>5</sup>, Masato Hasegawa <sup>6</sup>, Shen-Wen Chien <sup>7</sup> and Tzu-Sheng Shen <sup>7</sup>

<sup>1</sup> Division of Mechanical Science and Engineering, Graduate School of Natural Science and Technology, Kanazawa University, Kakumamachi, Kanazawa 9201164, Ishikawa, Japan

<sup>2</sup> 5th District HQs, Kaohsiung City Fire Bureau, Kaohsiung City 82150, Taiwan

<sup>3</sup> Fire Prevention Division, Kaohsiung City Fire Bureau, Kaohsiung City 80670, Taiwan

<sup>4</sup> Faculty of Production Systems Engineering and Sciences, Komatsu University, Nu 1-3, Shicho-machi, Komatsu 9238511, Ishikawa, Japan

<sup>5</sup> Graduate School of Advanced Science and Engineering, Transdisciplinary Science and Engineering Program, Hiroshima University, 1-5-1 Kagamiyama, Higashi-Hiroshima 7398529, Hiroshima, Japan

<sup>6</sup> Department of Mechanical Engineering, National Institute of Technology, Ishikawa College, Kitachujo, Tsubata 9290392, Ishikawa, Japan

<sup>7</sup> Department of Fire Science, Central Police University, Taoyuan City 33304, Taiwan

\* Correspondence: fc751126@gmail.com; Tel.: +886-953662519

**Abstract:** Japan and Europe have adopted significantly different ventilation modes with regard to traffic conditions (with or without congestion). This study focuses on the smoke behavior of different ventilation modes by conducting a 3D CFD analysis of smoke distribution and CO concentration variation and then comparing these modes based on two groups (relatively low target velocity: 0 and 1 m/s; relatively high target velocity: 2 and 3 m/s). The considered fire size is 30 MW for four longitudinal gradients (0, 2, 4, and 6%). In the simulation results, velocities of both 0 and 1 m/s reveal good performance in maintaining the stratification of smoke and ensuring the safety of the environment in 10 min in the occurrence of traffic jams. However, in 15 min, the smoke conditions change. Thus, it is difficult to distinguish which ventilation mode (0 and 1 m/s) shows relatively better performance during traffic congestion. When traffic is uncongested, the comparison of  $U_m = 2$  and 3 m/s reveals that a target velocity of  $U_m = 2$  m/s (lower than critical velocity) can also prevent the risk of smoke on the upstream side because no descending phenomenon is observed. Moreover,  $U_m = 2$  m/s causes the relatively slow propagation of descending smoke, increasing the possibility of evacuation once a second traffic incident occurs on the downstream side of the fire source.

**Keywords:** longitudinal ventilation; extinction coefficient  $C_s$ ; CO concentration; descending smoke



**Citation:** Tung, P.-W.; Chung, H.-C.; Kawabata, N.; Seike, M.; Hasegawa, M.; Chien, S.-W.; Shen, T.-S. Numerical Study of Smoke Distribution in Inclined Tunnel Fire Ventilation Modes Considering Traffic Conditions. *Buildings* **2023**, *13*, 714. <https://doi.org/10.3390/buildings13030714>

Academic Editors: Qi Zhang, Guozhu Zhang and Xiaobin Ding

Received: 6 February 2023

Revised: 1 March 2023

Accepted: 6 March 2023

Published: 8 March 2023



**Copyright:** © 2023 by the authors. Licensee MDPI, Basel, Switzerland. This article is an open access article distributed under the terms and conditions of the Creative Commons Attribution (CC BY) license (<https://creativecommons.org/licenses/by/4.0/>).

## 1. Introduction

In road tunnel design, ventilation systems are used to clean vehicle emissions and provide fresh air for the tunnel, providing safe high-speed transit. In an emergency such as a fire, ventilation systems effectively provide an evacuation environment by controlling smoke diffusion. Different ventilation methods (longitudinal, transverse, semi-transverse, and point extraction ventilation systems) have been applied to minimize human exposure to smoke. The longitudinal ventilation system is the most widely used system in Japan [1,2]. Around 95% of tunnels with ventilation systems (around 1100) adopt the longitudinal ventilation system in Japan [3].

In general, the international status of longitudinal fire emergency ventilation in unidirectional tunnels can be simply categorized by the following modes depending on the target velocity: (1) critical velocity ventilation; (2) low-speed ventilation; (3) zero-flow ventilation; and (4) shut-down ventilation [4,5]. Interestingly, the different adopted modes of Japan and Europe have significantly different effects with respect to traffic conditions.

In Japan, longitudinal velocity is mostly controlled at a state lower than critical velocity (around 2 m/s) in traffic without congestion and is controlled at zero-flow ventilation (around 0 m/s) in heavy traffic congestion [6,7]. The ventilation strategy of 2 m/s is considered a reasonable airflow that can moderately reduce the back-layering effects of smoke on the upstream side and maintain acceptable smoke propagation on the downstream side to increase the possibility of self-evacuation. Moreover, zero-flow ventilation applied in a unidirectional tunnel is based on the consideration of severe traffic congestion accompanying a traffic incident along with a secondary accident occurring with fire at the location of the first traffic accident, resulting in heavy jams both downstream and upstream of the fire source. People downstream of such a fire would not be able to leave the tunnel using their vehicles and would potentially need to participate in the evacuation and self-rescue process. This has been considered a critical issue in Japan. Hence, zero-flow ventilation is considered to improve the possibility of self-evacuation on both upstream and downstream sides of a fire source in this kind of scenario. Of course, this must be based on the precondition of rapid and early evacuation. However, whether zero-flow ventilation is achievable during real large-scale fires still requires investigation.

By contrast, in Europe, some countries control longitudinal fire ventilation velocity close to critical velocity ventilation (around 3–4 m/s) in traffic without congestion, and the mode changes to low-speed ventilation (around 1–1.5 m/s) when water spray is activated or when there is a heavy traffic jam [4,5]. In France, ventilation is operated in two stages in traffic with congestion if no localized massive smoke exhaust with a spacing of 500 m is installed. First-stage airflow velocity should be from 1 to 2 m/s to make self-evacuation possible, and in the second stage, it should be able to reach 3 m/s if required by firefighters [5]. PIARC [5] proposed principles for longitudinal ventilation in the self-rescue phase at relatively low velocities (e.g.,  $1.2 \pm 0.2$  m/s) in unidirectional traffic with congestion and applied an appropriate velocity to prevent or minimize the back-layering of smoke in unidirectional traffic without traffic congestion. As might be expected, ventilation strategies (target velocity) considering traffic with and without congestion also vary between European countries. The mode of velocity around 3–4 m/s is based on the goal of completely preventing smoke back-layering on the upstream side, as the vehicles on the downstream side can move faster than smoke propagation. The mode of velocity around 1–1.5 m/s is considered because the traffic conditions near the fire are not known in most cases. Relatively low target velocities can act as a compromise approach between “acceptable back-layering” and “acceptable smoke diffusion velocities downstream the fire” [8]. However, in Taiwan’s current practice, the tunnel ventilation mode does not consider the traffic congestion situation but only considers whether there are evacuees. Taking Taiwan’s longest tunnel, the Hsuehshan Tunnel (12.9 km, completed in 2006), as an example, its ventilation mode operates at the setting 2–4 m/s after the fire alarm system detects a fire and the situation turns into the evacuation model. When all the evacuees are safe, the ventilation mode changes to exhaust mode and activates all the jet fans to push out the smoke [9].

Moreover, the different considerations of the velocity of longitudinal ventilation modes of Japan and Europe are also related to fire scenario design. For road tunnels in Japan, tunnel fire strategy is based on the premise that tunnel users may safely complete evacuation in 10 min during a fire incident. Based on a fire test at No. 3 Shimizu Tunnel and the EUREKA EU499 tests, a maximum heat release rate (HRR) of 30 MW for a single large bus was confirmed [10–12]. These fire tests are widely adopted as a possible scenario in fire risk assessments in Japan. In Europe, due to the serious damage caused by the Mont Blanc and Tauern Tunnel fire accidents, much work has been undertaken to assess the risk of fire and possible fire scenarios. Moreover, the European Commission introduced Directive 2004/54/EC, which established a common ground for tunnel safety evaluation, providing certain minimum requirements while officially introducing the use of risk assessments [13]. Based on risk analyses representing scenarios related to experimental and statistical data, a series of fire scenario designs have been proposed. Assumed fire scales have ranged

from 10 MW to several hundred MW [12,14–16]. Typical critical velocities are estimated in the range of 2.2–3.5 m/s for fire scales of around 30–50 MW [8]. Since fire scales of over 30 MW have been considered in risk assessments, a forced velocity of at least 3 m/s is usually considered a criterion of longitudinal flow for preventing any upstream movement of smoke. Although the fire design of 30 MW in Japan seems relatively small compared with the fire scenarios considered in many European countries, the selection of fire scenario design (30 MW) in Japan mainly derives from the consideration of a strategy for completing evacuation within 10 min. In addition, when compared to a study of fire curve design in tunnels conducted by Ingason [14], a heat release rate of 30 MW in 10 min represents a reasonable fire scenario. Moreover, according to the fire statistics of tunnels of over 500 m from 1989 to 2011 in Japan, the proportion of fires caused by vehicle failure was 70.3%, and the proportion of fires caused by traffic accidents was 29.7% (single-vehicle accidents 14.5%, multiple-vehicle accidents 15.2%). A statistical fire risk assessment revealed that the potential fire risk based on fire scale is 21.3% for 0 MW (assuming a small-scale fire can be successfully extinguished in the early stage, it is shown as 0), 54.0% for 5 MW, 19.9% for 10 MW, 4.1% for 20 MW, and 0.7% for 30 MW [17]. Thus, it can be concluded that the long-term adoption of a fire scenario design of 30 MW in Japan is due to the purpose of tunnel fire safety assessment being mainly to invent strategies aimed at completing evacuation in 10 min rather than strategies for responding to a fire's scale in the firefighting (or rescue) phase. The assumption of the low possibility of a several hundred MW fire scale is based on past tunnel fire statistics. In Canada, when evaluating tunnel fire safety, 20 MW was assumed with respect to a bus fire [18]. In China, the most common vehicles in urban road tunnels are passenger cars or vans. The HRR for one passenger car or van is 5–15 MW [19]. In Taiwan's longest tunnel, the Hsuehshan Tunnel, a fire accident occurred that caused two deaths and 34 injuries in 2012. According to an analysis, the HRR of this fire was 25–30 MW, which was due to a bus and a wagon having caught on fire [9].

The longitudinal ventilation system is designed to control smoke propagation and maintain a tenable environment for evacuation, granting a region safe evacuation and available evacuation time before smoke descends significantly depending on the target velocity of different longitudinal ventilation modes. However, longitudinal ventilation is affected by natural draughts (natural ventilation, stack effect) due to the buoyancy forces in inclined tunnel fires [20]. Smoke movement is dominated by the stack effect [21], so smoke movement in inclined tunnel fires is different from that in horizontal tunnels [19]. It is therefore necessary to consider the slope in inclined tunnels. Moreover, target velocity is also dependent on several considerations, such as fire scale, design objectives, traffic conditions, longitudinal gradients, etc. Regarding traffic conditions, vehicular obstacles cause a blockage effect and decrease the need for critical velocity under the same HRR conditions. The back-layering length is additionally affected [7,22]. While the opinions regarding target velocity in fire emergency ventilation, especially considering traffic with and without congestion, the operational strategies of longitudinal ventilation modes still represent a complex issue that requires further investigation to gather more reliable scientific evidence in order to discuss the adequacy of such strategies. As reported in the literature, computational fluid dynamics (CFD) modeling is beneficial for comparing the consequences of different fire scenarios and evaluating the risk to road tunnel users. Consequently, many studies utilize CFD modeling and evacuation modeling in performing quantitative risk analysis (QRA).

Table 1 reviews the literature related to CFD simulation considering the ventilation modes of longitudinal ventilation systems. The above-cited literature revealed that a broad analysis of longitudinal velocity settings has been conducted. However, the analysis of longitudinal ventilation modes still needs to progress due to the insufficiency of full-scale systems with finer grid sizes regarding high-accuracy simulation for analyzing the descending smoke phenomenon. Moreover, examinations of the turbulence simulation capabilities of the CFD model are seldom mentioned even though turbulence simulation significantly affects smoke behavior far away from the fire source. These points are essential to reducing the gap between actual smoke distribution and simulation outcomes when performing QRA with high accuracy. To analyze the risk of evacuation safety, especially in considering tunnel users' evacuation under the smoke layer, the high-accuracy simulation of the descending smoke phenomenon in different longitudinal modes is indispensable. Nevertheless, about 70% of Japan and Taiwan is mountainous area and has complicated topography with steep mountains. In recent years, the tunnels connecting intra-urban expressways and inter-urban expressways have increased, and the traffic volume in tunnels has increased, making traffic jams more likely to occur. Moreover, tunnels with longitudinal gradients are not rare. Most of the tunnels in Taiwan are located in the eastern part of Taiwan, which is mainly mountainous. These tunnels connect urban areas and non-urban areas. Tunnels in mountainous areas have slopes, and smoke movement is affected by these slopes. Thus, we consider the inclination of tunnels as an important variable in this study. In addition, previous studies have mainly focused on the impact of tunnel slope on critical velocity [19]. Hence, the present study focuses on the descending smoke phenomenon in inclined tunnel fires. Excepting ventilation velocity, the inclination of tunnels is also considered a variable necessary for analyzing smoke distribution in the present study.

As such, to provide a more precise quantitative comparison of longitudinal ventilation modes based on the consideration of traffic with and without congestion, the present paper analyzes smoke distribution via a full-scale CFD model. The comparison of ventilation modes is based on the same fire scale of 30 MW commonly used in Japan and Europe. The analysis focuses on variants in the extinction coefficient  $C_s$  and CO concentration. The discussion of the ventilation modes focuses on safety regarding the environmental conditions of both sides near the fire source during the self-evacuation phase with and without traffic congestion. The fire simulation tool, tunnel model, and simulation conditions are described in Section 2. A discussion on the smoke distribution and CO concentrations in different ventilation modes is provided in Section 3. Section 4 further discusses the influence of gradients on smoke distribution. The merits, demerits, and limitations of the ventilation modes are summarized in Section 5. Finally, the findings and conclusions of this study are presented in Section 6.

**Table 1.** Simulation of full-scale tunnel fire considering the influence of longitudinal velocities, traffic conditions, and gradients.

	Caliendo et al., 2012 [23]	Caliendo et al., 2013 [24]	Nakahori et al., 2015 [6]	Kohl et al., 2017 [4]	Yamamoto et al., 2018 [25]	Khaksari et al., 2021 [26]	Na W. et al., 2022 [27]	Present Study
Simulation space	1200 m (L), 10.5 m (W), 5.5 m (H)	1200 m (L), 10.5 m (W), 5.5 m (H)	2990 m (L), cross-section 71 m <sup>3</sup>	3032 m (L), cross-section 50.4 m <sup>3</sup>	700 m (L), 9.6 m (W), 5.4 m (H)	1800 m (L), 7.3 m (W), 5.2 m (H)	1000 m (L), 12 m (W), 8 m (H)	2200 m (L), 11 m (W), 6.8 m (H)
Grid sizes	1×1×1 m <sup>3</sup> (near fire) 3.5×3×2.5 m <sup>3</sup> (rest)	1×1×1 m <sup>3</sup> (near fire) 1.5–4 m (far from fire)	2D simulation (no grid size information)	1D and 3D Simulation (no grid size information)	–	0.2 (or 0.25)×0.2×0.25 m <sup>3</sup> (in fire section 40 m) 0.5×0.2×0.25 m <sup>3</sup> (rest)	0.4×0.4×0.4 m <sup>3</sup>	0.33×0.24×0.19 m <sup>3</sup> (–1100 m–1100 m)
Fire scales	50 MW	8, 30, 50, 100 MW	30 MW	5, 30, 100 MW	30 MW	5 and 100 MW	50 MW	30 MW
Traffic conditions	Without congestion but with vehicles	Without congestion but with vehicles	Both with and without congestion	Both with and without congestion	Without congestion	With congestion	With congestion	Both with and without congestion
Ventilation velocities	6–13 m/s	9 m/s	Zero-flow ventilation (0 m/s), shutdown mode	0, 1.5, 3 m/s, shutdown mode	0, 0.5, 1.0 m/s	Shutdown mode	0, 1, 2, 4.5, 6 m/s	0, 1, 2, 3 m/s
Longitudinal gradients	2%	2%	±2%	A tunnel with 4 gradients (–6, 2.6, 0.3, and 3.5%)	1.11%	4%	–5, 0.5, 4%	0, 2, 4, 6%
Simulator	CFX code	CFX code	Tunnel safety simulator/TuRisMo2	FDS	FDS (version 5.5.3)	FDS + Evac (version 6.7.5)	FDS + Pathfinder (version 6.7.5)	Fireles
Smagorinsky coefficient (verification of turbulence reproducibility)	N/A	N/A	N/A	0.2* (N/A)	0.2* (N/A)	0.2* (N/A)	N/A	0.14 (Yes)
Turbulence reproducibility examination	–	–	–	–	–	–	–	Examine friction factor and turbulence intensity

\* Fire Dynamic Simulator (FDS) versions 1 through 5 also adopted the Smagorinsky coefficient with the default value of 0.20 but adds the dynamic Smagorinsky model currently.

## 2. Numerical Calculation and Accuracy Confirmation

In the present study, we executed our self-developed 3D CFD code (Fireles) [28] using large eddy simulation (LES) as the turbulence (standard Smagorinsky) model. As governing equations of the heat and airflow in the tunnel, the continuity equation, momentum equation, equation of energy conservation, equation of state, and equation of smoke concentration were used (see the Appendix A for details). In the spatial schemes, the momentum equation was discretized by a fourth-order central-difference scheme, and the energy and smoke-concentration equations were discretized as third-order and first-order upwind-difference schemes, respectively. Other spatial differentials were discretized as second-order central-difference schemes. Combustion reactions were not considered in the present CFD model. Instead, we represented heat release and smoke generation as source terms in the energy and concentration equations, respectively, thereby treating fire as a heat and smoke source. Smoke behavior simulation capabilities in Fireles were confirmed by comparing the numerical results with experimental results from both model-scale and full-scale tunnels [7,28–36]. A validation of the related parameters and index from previous experiment studies performed using the 3D CFD code (Fireles) is shown in Table 2.

**Table 2.** Validation of related parameters from previous experiment studies in Fireles.

Validation Item (Parameter)	Validation Reference
Heat release rate	Kawabata et al., 1998 [28]
	Kunikane et al., 2002 [10]
	Kunikane et al., 2003 [11]
	Kunikane et al., 2003a [30]
	Kikumoto et al., 2007 [34]
Seike et al., 2019 [35]	
Smoke generation rate	Kunikane et al., 2002 [10]
	Kikumoto et al., 2007 [34]
	Seike et al., 2014 [33]
Fire plume behavior	Kunikane et al., 2003a [30]
Back-layering	Wang Q. et al., 2000 [29]
	Ho et al., 2022 [7]
Temperature distribution	Kunikane et al., 2002 [10]
	Kunikane et al., 2003 [11]
	Kikumoto et al., 2007 [34]
Turbulence intensity	Ho et al., 2022 [7]
Vehicular blockage effect	Ho et al., 2022 [7]
Descending smoke phenomenon	Kawabata et al., 2003a [36]
Chimney natural exhaust effect	Yokota, M. et al., 2012 [32]
Water Spray	Kawabata et al., 2004 [31]

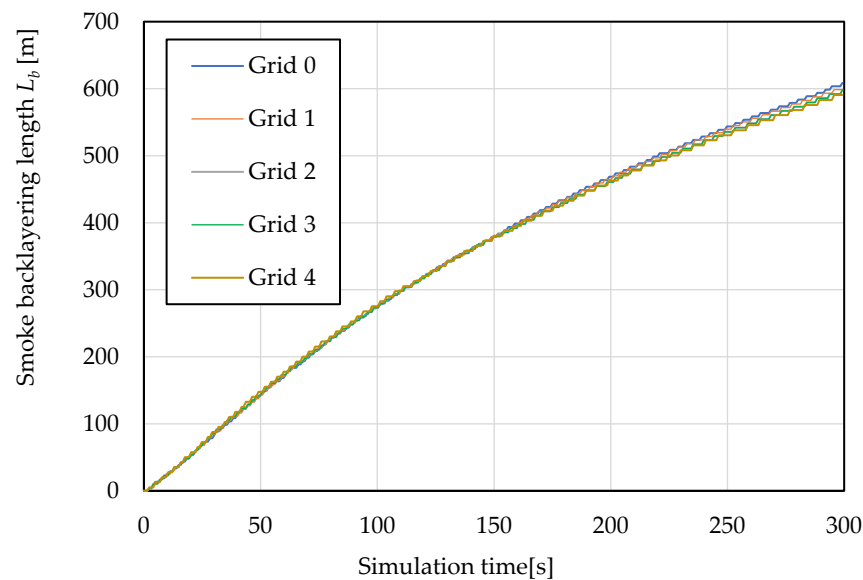
### 2.1. Grid independence Analysis by Comparing the Back-Layering Length

Since the reproducibility of smoke back-layering lengths is dependent on grid size, we conducted a grid independence analysis before the formal simulation. The simulation space for the grid analysis was 1000 m in length, 11 m in width, and 6.8 m in height with one portal closed. The average longitudinal velocity ( $U_m$ ) was set at 0 m/s. The heat generation rate was set to reach 10 MW (corresponding to the 20 MW convection heat in conditions where two side portals are open) at 30 s and to then keep the HRR steady. The simulation performance duration was from the start of heat generation until 300 s had elapsed. The grid divisions are detailed in Table 3.

**Table 3.** Specifications of grid sizes.

	Grid 0	Grid 1	Grid 2	Grid 3	Grid 4
Number of grids in the x-direction	3000	2800	2400	2200	2000
Number of grids in the y-direction	45	41	37	35	33
Number of grids in the z-direction	35	33	29	27	25
$\Delta x, \Delta y, \Delta z$ (m)	0.333, 0.244, 0.194	0.357, 0.268, 0.206	0.416, 0.297, 0.234	0.455, 0.314, 0.252	0.500, 0.333, 0.272
$\sqrt[3]{\Delta x \Delta y \Delta z}$ (m)	0.251	0.270	0.307	0.330	0.357
Total mesh number	4,396,145	3,542,969	2,441,553	1,987,255	1,598,567

Figure 1 shows the simulation results for the smoke back-layering lengths of four grid sizes. Smoke back-layering length significantly increased after ignition as the fire source built up to a steady state in a short time. The difference in back-layering lengths between the four grid sizes was not significant. When further analyzing the deviation based on the benchmark of back-layering length in the case of Grid 0 (Equation:  $|L_b - L_{bGrid0}|/L_{bGrid0}$ ), the deviation of the average back-layering length with a simulation time of 285–300 s was 0.87% for Grid 1, 1.66% for Grid 2, 1.7% for Grid 3, and 2.38% for Grid 4. The deviation of back-layering lengths for the four grid sizes was small (an error of no more than 5%). Furthermore, high-accuracy simulation results are necessary for high-accuracy discussions of the CO concentration and smoke distribution in this study. Based on the above analysis, we chose Grid 0 to conduct the simulation in this study.

**Figure 1.** Smoke back-layering length  $L_b$  with simulation time.

## 2.2. Verification of Turbulence Reproducibility

In our 3D computational fluid dynamics (CFD) code, the LES model was applied to simulate the turbulence flow. The sub-grid scale model formulated in LES was originally established by the Smagorinsky model and expressed as the following function.

$$\nu_t = (C_{sgs}\Delta)^2 \left\{ \frac{1}{2} \left[ \frac{\partial v_i}{\partial x_j} + \frac{\partial v_j}{\partial x_i} \right]^2 - \frac{2}{3} (\nabla \cdot \mathbf{v})^2 \right\}^{\frac{1}{2}} \quad (1)$$

Here,  $\nu_t$  is the turbulent kinematic viscosity coefficient.  $C_{sgs}$  is the Smagorinsky coefficient which depends on the type of flow;  $\Delta$  is the size of the filter and is given by  $(dx dy dz)^{1/3}$ ; and  $v$  is the velocity vector.

Because of its sensitivity, the constant  $C_{sgs}$  is an important parameter. Although a Smagorinsky coefficient of 0.20 is considered suitable for application in tunnel fires as the fire region is the driving force behind changes in the forced flow conditions [37], a greater value would result in the loss of the large-scale eddy component dynamics because the turbulent kinematic viscosity coefficient of small-scale eddies increases and causes a reduction in the generation of eddies larger than the filter size. The Fire Dynamic Simulator (FDS) versions 1 through 5 also adopted the Smagorinsky coefficient with the default value of 0.20 but adds the dynamic Smagorinsky model currently. The coefficient  $C_{sgs}$  is not necessarily taken as a constant but rather is computed based on local flow conditions [38]. Considering the importance of  $C_{sgs}$  for turbulence modeling, we adjusted the Smagorinsky coefficient and then examined the turbulent simulation capability of the present LES model.

Regarding the examination of the turbulent simulation capability, we took the approach mentioned in the study by Kawabata et al. [39] as a reference and focused on pressure loss in the turbulence flow.

When fluids flow through pipes, energy losses inevitably occur. One cause of this is friction that occurs between the pipe wall and the fluid (wall friction). Further flow energy losses are caused by turbulences in the fluid. The friction and flow effects described above are therefore accompanied by a corresponding pressure loss. Furthermore, pressure loss (pressure drop) through a pipeline can be reflected by the friction factor ( $\lambda$ ) according to the Darcy–Weisbach equation [40]. Thus, it can be concluded that variance in the friction factor ( $\lambda$ ) can indicate the turbulent state of the fluid but cannot further exclude the effect of wall friction on pressure loss. As a result, we first examined friction factor  $\lambda$  to grasp the total pressure loss in the simulation results. We then further examined turbulence intensity (related to the component of energy loss from turbulence) to confirm turbulent simulation capability.

The examination of the LES model simulation capability was performed in normal ventilation conditions before conducting the fire simulation. The simulation space was a tunnel of 500 m in length (assume the length was sufficient to reach the completed turbulent flow), 11 m in width, and 6.8 m in height. The wall roughness was assumed to be 7 mm. The longitudinal flow inlet was set at  $x = 500$  m and the outlet was set at  $x = 0$  m. The average velocity of the cross-section ( $U_m$ ) was set at 1 m/s (Reynolds number =  $6.0 \times 10^5$  close to a state of turbulent flow). The longitudinal flow inlet was set at  $x = 500$  m, and the outlet was set at  $x = 0$  m. To ensure that a turbulent flow was produced, blockages were set up 7 m from the flow inlet in the simulation.

Table 4 shows the simulation results for different  $C_{sgs}$  values.  $u_c$  means the velocity in location  $y = 0$  m and  $z = 3.2$  m along the  $x$ -axis. Average velocity ( $\bar{u}_c$ ) indicates a well-developed turbulent state after simulation times over 1140 s. The calculation of  $\bar{u}_c$  in Table 4 was conducted via time-average and space-average calculations. We took the mean within 60 s at a simulation time of 1140–1200 s and then further took the average of the time-averaged velocity in the region of  $x = 50$ –200 m. Each  $C_{sgs}$  and the corresponding friction factor ( $\lambda$ ); the average velocity ( $\bar{u}_c$ ) at the center of the cross-section; the RMS (root mean square) value of the fluctuation component of velocity in the  $x$ -direction ( $\sqrt{u'^2} = \sqrt{(u_c - \bar{u}_c)^2}$ ); and the turbulence intensity of the eddy scale larger than the grid size ( $\sqrt{u'^2}/\bar{u}_c$ ) are listed.

**Table 4.** Simulation results of Smagorinsky coefficient ( $C_{sgs}$ ).

$C_{sgs}$	Um [m/s]	Friction Factor $\lambda$	Average Velocity $\bar{u}_c$ [m/s]	Turbulence Intensity $\sqrt{u'^2}/\bar{u}_c$ [-]
0.09	1.0		Unstable	
0.10	1.0	0.0156	1.23	0.0297
0.11	1.0	0.0148	1.23	0.0267
0.12	1.0	0.0144	1.21	0.0282
0.13	1.0	0.0144	1.22	0.0290
0.14	1.0	0.0145	1.21	0.0353
0.15	1.0	0.0149	1.19	0.0361
0.16	1.0	0.0096	1.30	0.0055
0.17	1.0	0.0104	1.28	0.0038
0.18	1.0	0.0106	1.30	0.0022
0.20	1.0	0.0112	1.29	0.0006

There was a significant difference between  $C_{sgs}$  smaller than 0.15 and larger than 0.16. When  $C_{sgs}$  was in the range of 0.10–0.15, friction factor

There was a significant difference between  $C_{sgs}$  smaller than 0.15 and larger than 0.16. When  $C_{sgs}$  was in the range of 0.10–0.15, friction factor  $\lambda$  was around 0.0144–0.0156,  $\bar{u}_c$  was around 1.2 m/s, and the turbulence intensity was 0.0297–0.0361. When  $C_{sgs}$  was over 0.16, friction factor  $\lambda$  was around 0.0096–0.0112,  $\bar{u}_c$  was around 1.28–1.3 m/s, and the turbulence intensity was 0.0006–0.0055.

Comparing the Blasius empirical equation, the friction factor of 0.0096–0.0112 was relatively close to the value from the equation of the turbulence flow in the smooth pipe ( $\lambda = 0.316/Re^{1/4} = 0.0113$ ) [41]. There was clearly a physical inconsistency, because the full-scale tunnel should be a relatively rough pipe rather than a smooth pipe. However, the friction factor  $\lambda$  of full-scale tunnels has been reported as 0.016 to 0.036 [42]; in actual tunnels, there are various installations which can increase friction resistance in addition to surface roughness. Thus, it can be said that  $C_{sgs}$  of 0.15 or less is appropriate because of friction factor  $\lambda$ .

Turbulence intensity significantly decreased when  $C_{sgs}$  was over 0.16. Almost no turbulence intensity on the eddy scale larger than the grid size can be observed in the simulation results, even where blockages were set up 7 m away from the flow inlet to ensure a turbulent state. Moreover, the value of  $\bar{u}_c$  in different  $C_{sgs}$  conditions in Table 4 implies that the shape of the velocity distribution flattened rather than becoming more parabolic in cases where  $C_{sgs} = 0.10$ –0.15, which had relatively greater turbulence intensity than in cases where  $C_{sgs} = 0.16$ –0.20. It is thought that the velocity distribution shape becomes flat due to the stirring effect of the turbulent eddies. Furthermore, comparing the turbulence intensity investigation of past experiments illustrated by Kawabata et al., (2003), [39], the turbulence intensities of 0.0267–0.0361 in cases of  $C_{sgs} = 0.10$ –0.15 as reported in Table 4 are relatively close to the turbulence intensities of 0.03–0.05 reported in past experiments (in the condition  $Re = 6.5 \times 10^4$ ,  $8.3 \times 10^4$ , and  $2.5 \times 10^5$ ) on square duct flow [39].

Thus, when performing the calculation of the present CFD code, a  $C_{sgs}$  set larger than 0.16 would result in low performance in turbulence reproducibility. Additionally, the simulation would be unstable with a  $C_{sgs}$  of 0.09. Based on the above analysis, we decided to set  $C_{sgs}$  to 0.14 in this study.

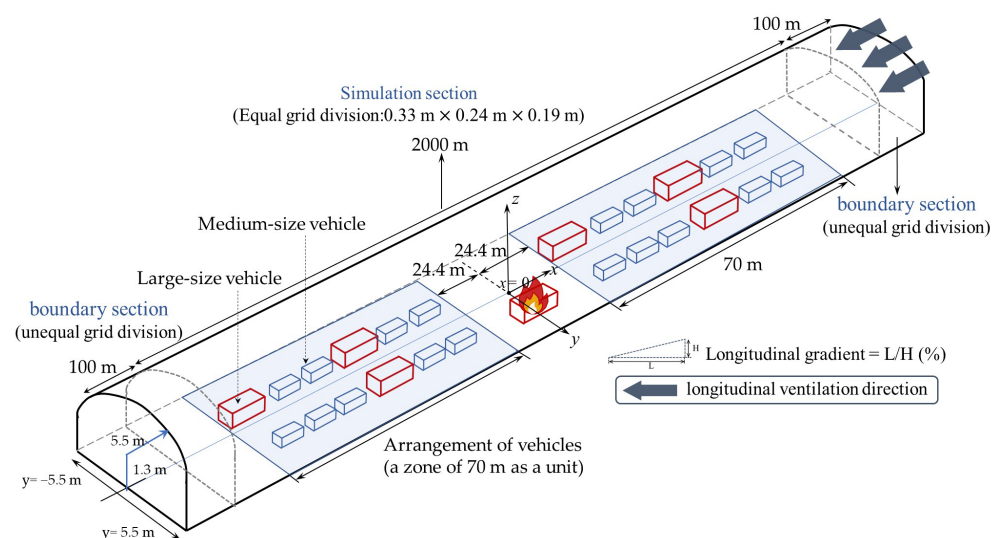
Another calculation setting of the present CFD code (Fireles) excluding the  $C_{sgs}$  value is shown in Table 5.

**Table 5.** Calculation setting of the simulator.

Calculation constant		Courant number: 0.2 Smagorinsky coefficient: 0.14 Turbulent Prandtl number: 0.7 Turbulent Schmidt number: 0.7
Boundary conditions	The surface of a wall	Velocity: logarithmic law of roughness Temperature: heat transfer coefficient [43]
	+x inlet	Uniform wind velocity
	−x inlet	Constant pressure
Calculation scheme		Velocity: fourth-order central-difference scheme Temperature: third-order upwind-difference scheme Smoke: first-order upwind-difference scheme Condition in the wall: 1D heat conduction equation

### 2.3. Simulation Conditions of the Large-Scale Tunnel

The simulation tunnel in this study was 2200 m in length, 11 m in width, ( $y$ -coordinate =  $-5.5$ – $5.5$  m), and 6.8 m in height ( $z$ -coordinate =  $0$ – $6.8$  m) (see Figure 2). To completely calculate the area of smoke distribution, the  $x$ -coordinate of the calculation space was adjusted according to simulation cases, but the size of the calculation space was fixed.

**Figure 2.** Cross-section and schematic diagram of the simulation tunnel.

The wall material was concrete, the specific heat was  $879$  [J/(kg·K)], the density was  $2100$  [ $\text{kg}/\text{m}^3$ ], and the thermal conductivity was  $1.10569$  [ $\text{W}/\text{m}\cdot\text{K}$ ]. The thickness of the wall was  $175$  [mm] and divided into nine divisions (the division is unequal). On the other hand, Kawabata et al. [39] reported that the division size where closest to the inside of the wall suitably set at the order of around  $1$  mm for thermal conductivity reproducing. In the present study, the division size where closest to the inside of the wall was  $2.33$  [mm], which was also close to the order of the previous study.

Two vehicle lanes were assumed. The tunnel construction was assumed to be concrete. The longitudinal gradient was based on the left side of the tunnel portal with conditions of  $0$ ,  $2$ ,  $4$ , and  $6\%$ .

In the simulation space, the arrangement of vehicles was repeated with a zone of  $70$  m as a unit. The ratio of large vehicles (truck, bus) was assumed to be  $25\%$  (see Figure 3). The total congested vehicles was around  $342$  (some deviations depending on the simulation case). However, the occurrence of accidents blocks traffic, and jams start to form [44]. Non-congestion conditions soon become congested on the upstream side of the fire source.

Furthermore, a vehicle's deployment will influence smoke behavior and the back-layering length [7]. Thus, this study deployed the same vehicles in both congestion and non-congestion conditions to distinguish the difference between each ventilation mode. Two vehicle sizes were considered (medium size and large size). Vehicles were assumed to be rectangular obstacles, and the gap to the road surface was ignored. The height and width of the vehicle model were set in consideration of the ease of grid division. This study refers to the  $C_d$  value to roughly match various vehicles in the real world for calculating smoke behavior in tunnel fires so that the simulation results may be closer to those of a real situation. We compare the  $C_d A$  values of real-size and model-size vehicles in Table 6. The  $C_d A$  value is the multiplication of the air drag coefficient ( $C_d$ ) and frontal projected area ( $A$ ), which is used as one of the parameters that indicates the performance of automobiles. In further considering that the resistance coefficient of an object stationary on the floor is 0.2 to 0.3 less than that of an object (square with rounded corners) in the air (about 1.2), the  $C_d$  values of the model were set to 0.84 and 0.96. Two  $C_d$  values are provided because the  $C_d$  value differs depending on vehicle type. The actual sizes of the medium-sized and large-sized vehicles and the  $C_d A$  values of the models roughly matched.

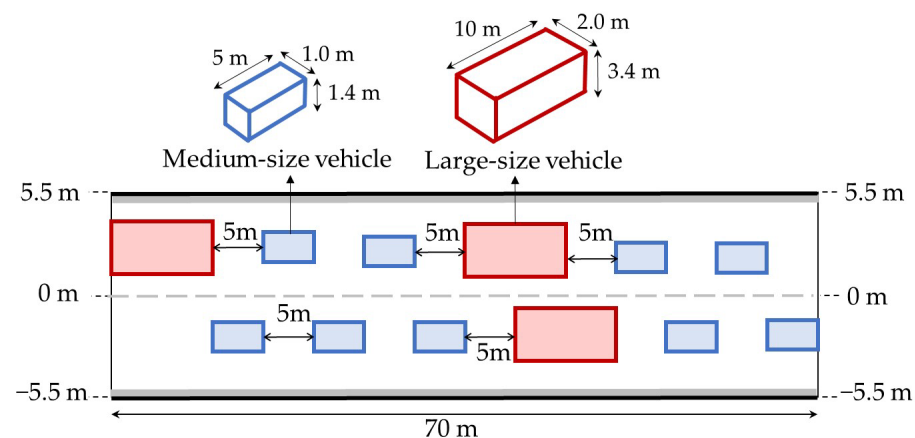


**Figure 3.** Arrangement of vehicles.

**Table 6.** Comparison of actual and model-size vehicles.

	Large-Sized Vehicle		Medium-Sized Vehicle	
	Real	Model	Real	Model
Length [m]	10	10	4.8	5.0
Width [m]	2.5	2.0	1.7	1.0
Height [m]	3.5	3.4	1.7	1.4
Volume [m <sup>3</sup> ]	75	68	12.2	7.0
Frontal projected area [m <sup>2</sup> ]	7.5	6.8	2.55	1.4
$C_d$ [-]	0.8	0.84/0.96	0.5	0.84/0.96
$C_d A$ [m <sup>2</sup> ]	6.0	5.7/6.5	1.1	1.2/1.3

Note: Height from the tunnel floor to the bottom of the vehicle (large-sized vehicle: 0.5 m; medium-sized vehicle: 0.2 m) was excluded when calculating the volume and frontal projected area of the real-size vehicle.

The heat generated from the fire source mainly consisted of the convection of hot flow and heat absorbed by the smoke and walls due to the radiant heat. The smoke particles were heated by radiant heat near the fire source. However, the ceiling wall was heated by the radiant heat of the smoke particles, which represents a very complicated heat exchange phenomenon. Since it is difficult to reproduce these phenomena by simulation, only the convective component is given as the heat generation rate in this study. It is noted that in full-scale experiments in Europe and Japan, it is common for convective components to account for 70% and 60% of the total heat generation rate, respectively [12].

The assumed fire scale in this study was 30 MW (assuming 60% convective HRR, quadratic fire growth rate  $\alpha = 0.08 \text{ kW/s}^2$ ). Figure 4 shows the change in the convective HRR and smoke generation rate with time. The fire source was assumed to be a heat generation area simulating the shape of the vehicle in taking the study by Huang et al., and the EUREKA 499 fire experiment as references [1,2]. As the fire developed, the heat generation area gradually enlarged, and the curve grew with the tendency of the time square until 480 s, then remaining constant after 480 s. The smoke generation rate was assumed to be the same as the HRR curve with the tendency of the time square. The smoke generation rate reached 90 g/s in 480 s, after which the smoke generation rate was constant. All the settings of the simulation conditions are listed in Table 7.

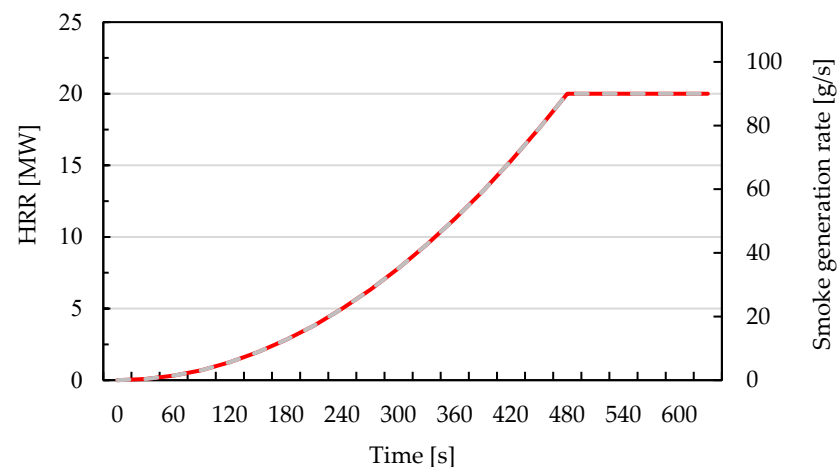


**Figure 4.** Convective HRR and smoke generation rate.

**Table 7.** Simulation condition settings.

Simulation Tunnel	2200 m (L) × 11 m (W) × 6.8 m (H)
Grid size	0.333 m × 0.244 m × 0.194 m
Total grid number	8,821,739
Heat release rate (HRR)	30 MW (convective HRR = 20 MW)
Vehicle number	Around 342 (with an interval of 5 m, 75% of Medium size, 25% of large size)
Longitudinal ventilation	0, 1, 2, 3 m/s
Longitudinal gradient	0, 2, 4, 6%
Simulation time	900 s

#### 2.4. Smoke Distribution Assessment

Smoke distribution is a critical factor considered in the quantitative risk assessment (QRA) of tunnel fires [15,16,45,46]. Tunnel quantitative risk assessments in Japan often consider the notion that when a fire occurs in a tunnel, evacuees' walking speeds decrease due to the obstruction of their visibility by smoke, increasing the risk of incapacitation. Thus, we focus on an analysis of smoke distribution in the present study to discuss the safety of the evacuation environment using the extinction coefficient  $C_s$  [ $\text{m}^{-1}$ ], which is an index of smoke density. The concentration of smoke ( $C_s$ ) is a measurement of optical smoke density widely used in studies on tunnel fires and is used to measure smoke density in this study.  $C_s$  density was averaged based on tunnel width and was calculated as an extinction coefficient in the Lambert–Beer equation as follows:

$$C_s = -\frac{1}{l} \ln\left(\frac{I}{I_0}\right) \quad (2)$$

where  $I$  is the intensity of incident light,  $I_0$  is the intensity of transmitted light (non-smoke), and  $l$  is the distance traveled by light through the gas.

In the CFD analysis, various physical quantities are calculated by the governing equation based on the conservation law. Thus, smoke density solved via CFD analysis also needs to follow conservation law, but extinction coefficient  $C_s$  does not have a conservation law. The mass concentration of soot yields ( $M$ ) [ $\text{g}/\text{m}^3$ ] of smoke particles with preservability is therefore obtained by CFD analysis, and  $M$  is converted to  $C_s$  by the conversion equation (Equations (2) and (3)) of mass concentration  $M$  and extinction coefficient  $C_s$  based on experiments [33,47].

$$C_s = 10M, M \leq 0.26 \text{ [g/m}^3\text{]} \quad (3)$$

$$C_s = 1.73 \ln(M) + 4.94, M > 0.26 \text{ [g/m}^3\text{]} \quad (4)$$

In addition, experiments on evacuation speed in smoke-filled tunnels have shown that the average walking speed of evacuees decreases when the  $C_s$  concentration increases [48–50], and  $C_s = 0.4 \text{ m}^{-1}$  has usually been considered as the standard in road tunnel fire risk assessment in Japan [1,2]. A visibility distance of 10 m is also widely used as the acceptable safety criterion for tunnel user survival in case of fire [12,51]. According to the function of visibility distance [ $\text{m}$ ] =  $(2-4)/C_s$  for a reflecting sign [52], the extinction coefficient  $C_s$  converted by a visibility distance of 10 m is  $C_s = 0.2-0.4 \text{ m}^{-1}$ . Thus, safety criteria for evaluating the hazard of smoke through the viewpoint of an extinction coefficient or visibility distance are similar. As a result, this paper analyzes the hazard of smoke diffusion based on the criteria of  $C_s = 0.4 \text{ m}^{-1}$  at the 1.8 m eye level.

### 2.5. CO Concentration Assessment

The contention that a zero-flow ventilation mode is unsuitable for application in fire ventilation is due to the fact that local concentrations of toxic gases as well as the local temperature can increase significantly and in turn dramatically reduce the tenability of life and safety near a fire zone. Thus, excluding the extinction coefficient ( $C_s$ ), we also investigated the distribution of CO concentration for the discussion of different longitudinal ventilation modes.

CO gas is a critical component in the widely used fractional effective dose (FED) model [53] for estimating incapacitation or death when evacuees are exposed to toxic gas. In the present study, the CO generation rate is assumed proportional to the fire growth rate and smoke generation rate for 480 s and then stays at a constant generation rate. For the condition of a fire scale of 30 MW with longitudinal ventilation, the constant CO generation rate is assumed to be 108 g/s [54].

In turn, longitudinal air flow is considered to reduce the CO yield and typically dilutes the smoke stream, so a larger ventilation velocity would result in lower CO volume concentrations. Reduced-scale experiments investigating the influence of longitudinal velocities on CO concentration have reported that the ratio of CO concentration in conditions without longitudinal ventilation to that in conditions with longitudinal ventilation (0.4 m/s, 0.8 m/s, and 1.2 m/s) is around 3:1 [55]. As such, we take Yang et al., (2011)'s experiment as a reference to further assume that the CO generation rate without longitudinal ventilation would be three times the CO generation rate with longitudinal ventilation. However, it should be noted that the ratio of CO concentration in conditions with and without longitudinal ventilation is also simultaneously influenced by temperature rise. Thus, the present proportional parameter setting for CO concentration is still relatively rough.

Regarding the acceptable level of CO exposure, various reference concentrations in experiments have indicated its hazard to the human body. The Acute Exposure Guideline Levels (AEGs) for Hazardous Substances pointed out that CO concentrations of 1700 ppm within 10 min, 600 ppm within 30 min, and 330 ppm within 60 min are considered to result in life-threatening health effects or death [56]. On the other hand, the Immediately Dangerous to Life or Health Concentrations (IDLH) values report CO concentration as immediately dangerous at 1200 ppm [57], and this value is also used as a suitable safety

criterion for tunnel users [23,24,51]. Since the toxic gas of tunnel fires is not only CO, a CO concentration lower than the lethal concentration is usually taken as the basis for determining the acceptable criteria. To simplify the discussion on CO exposure risk, we chose 1200 ppm, 600 ppm, and 330 ppm as reference values which reflect the hazard of long- or short-term CO exposure and compared them to the CO concentration of the simulation results. This analysis of CO concentration focused on cases of tunnels without gradients and at the 1.8 m eye level. The results are shown in Section 3.

### 3. Longitudinal Ventilation Mode Comparison

To assess whether longitudinal ventilation can maintain evacuation conditions, we illustrated the simulation results under different longitudinal ventilation modes. The results of smoke distribution were compared for two groups of cases with low ( $U_m = 0$  and 1 m/s) and high ( $U_m = 2$  and 3 m/s) ventilation which we referred to as congested and uncongested conditions, respectively. To better clarify the distribution and direction of the smoke, we denoted the smoke layer moving toward the upstream side of the fire source as smoke back-layering; the smoke layer moving toward the downstream side of the fire source as smoke propagation; and the smoke moving toward the road surface as descending smoke. The discussion on the smoke environment affecting evacuation safety was based on two situations, the first being the self-evacuation phase (evacuation evaluation time of 10 min) and the second being evacuation delay (evacuation evaluation time expands to 15 min). Since there are vehicles both upstream and downstream of the fire source in the condition of traffic with congestion, the discussion on evacuation safety considered both upstream and downstream sides.

#### 3.1. Velocities 0 and 1 m/s for the Consideration of Traffic Congestion

Figure 5 illustrates the smoke distribution (Cs) of the central longitudinal section ( $y = 0$  m). The range of  $x$  is the total length of the simulation section of 2200 m, and the fire source is located at  $x = 0$  m. The range of  $x$  was set to  $x = -1100$ – $1100$  m in the case of a longitudinal velocity (denoted as  $U_m$  in the following content) of 0 m/s and was set to  $x = -1600$ – $600$  m in the case of  $U_m = 1$  m/s depending on the spreading of smoke. The longitudinal gradient was 0%. The time illustrated in Figure 5 is an average time within 30 s.

The  $U_m = 0$  m/s in the vicinity of the fire source was maintained by using jet fans away from the fire source (called the “zero-flow-control”) [1,2,6]. As shown in Figure 5, the generated high-temperature smoke behavior depended only on its buoyant forces without external influences near the fire source. The smoke rose to the ceiling and propagated upstream and downstream along its away from the fire. The back-layering significantly extended to the upstream side due to low resistance from the longitudinal flow. The smoke stratification was maintained well for 10 min. After 10 min, the turbulent smoke around the fire source was gradually diffused, and the destroyed smoke layer descended toward the road surface in the region of  $x = \pm 200$  m at 13 min and expanded to  $x = \pm 500$  m at 15 min.

When  $U_m = 1$  m/s, the back-layering length on the upstream side gradually extended within 9 min and was maintained at around 300 m from the fire source until 15 min. This length was significantly shorter than that in the case of  $U_m = 0$  m/s, where back-layering extended to around 800 m from the fire source. Clear smoke stratification on the downstream side could be observed within 10 min. After 10 min, the turbulent smoke diffused toward the tunnel road in the region of  $x = -600$ – $-700$  m at around 13 min and expanded to  $x = -600$ – $-1000$  m at 15 min. The distance and mean velocity of smoke propagation on the downstream side were 1300 m and 1.44 m/s, respectively, which was relatively fast compared with the longitudinal velocity.

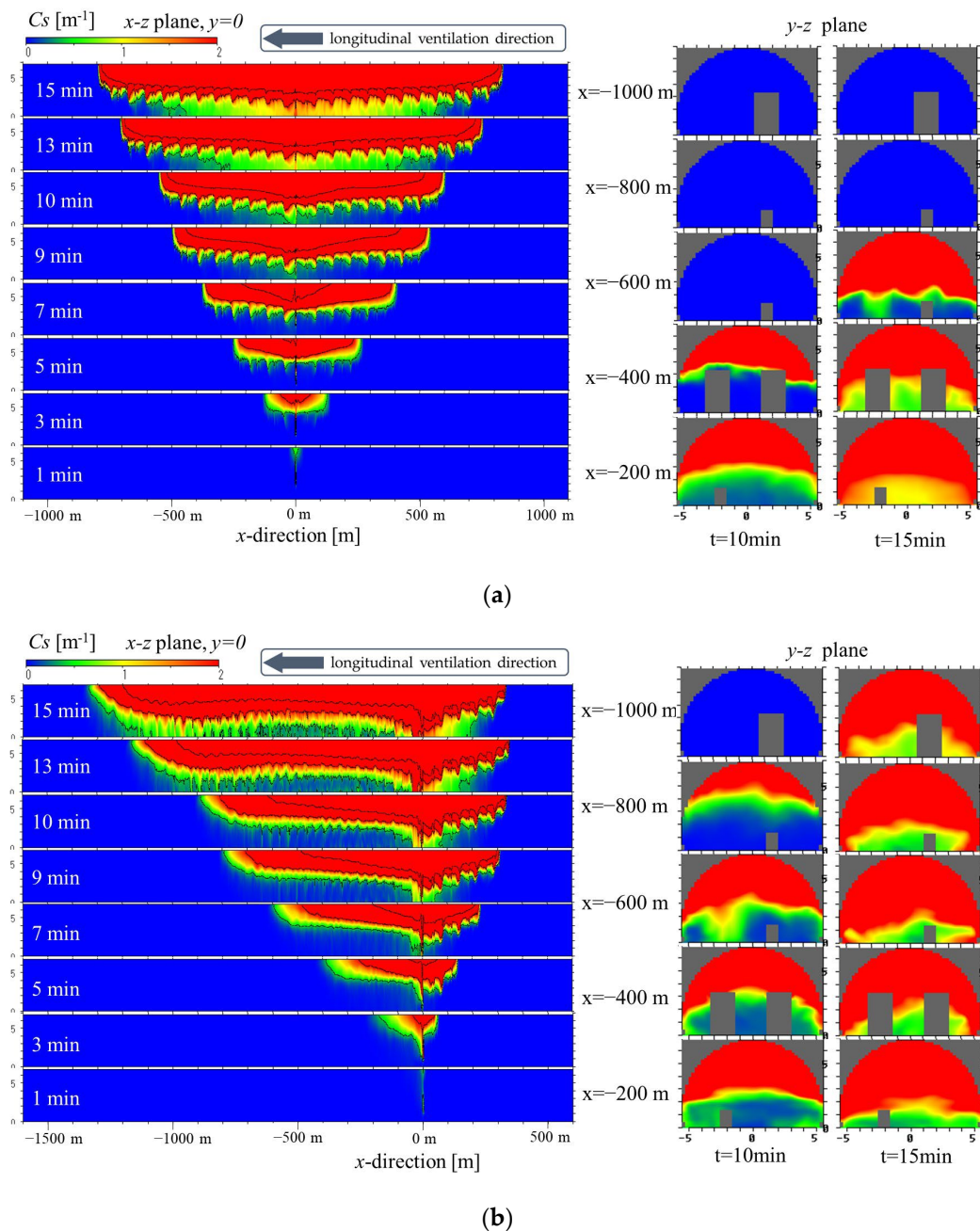


**Figure 5.** Side view of smoke distribution with  $U_m = 0$  and  $1$  m/s. (a)  $0$  m/s; (b)  $1$  m/s.

In general, even if smoke back-layering were to occur, this smoke would not cause immediate harm to evacuees if it maintained a stratification state near the tunnel ceiling; that is, the harm of smoke to evacuees depends on whether exposure to smoke results in their speed decreasing or in them being unable to move, and this factor is strongly related to the descending phenomenon of turbulent smoke. Thus, we also analyzed the smoke descending region and corresponding descending time to grasp the hazard of smoke descending on the environment for safe evacuation (see Figure 6). Moreover, the criterion for smoke density rests in considering the extinction coefficient  $C_s = 0.4 \text{ m}^{-1}$  descending to the height of  $1.8 \text{ m}$  per  $100 \text{ m}$  from the fire source, i.e., whether the smoke has reached head height and affected people's evacuation.

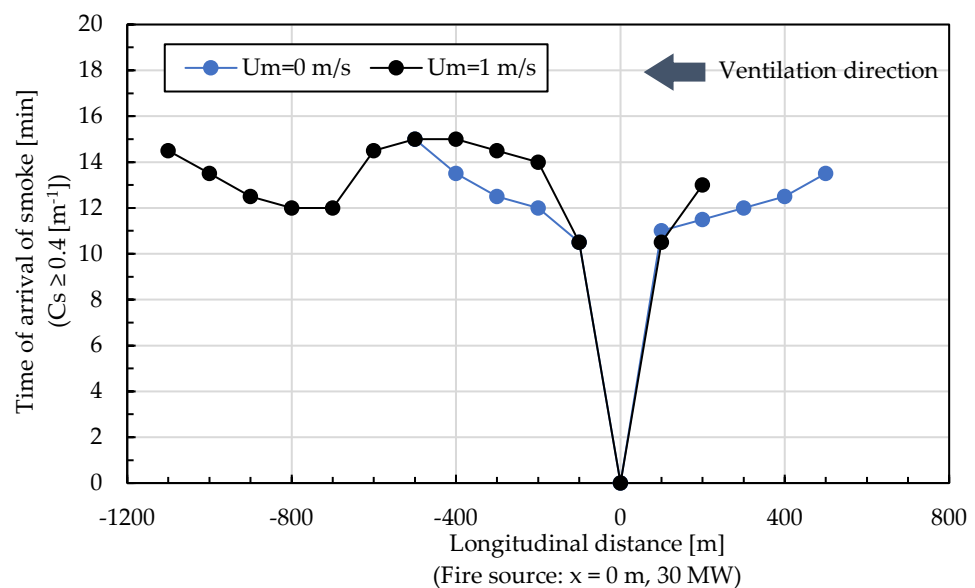
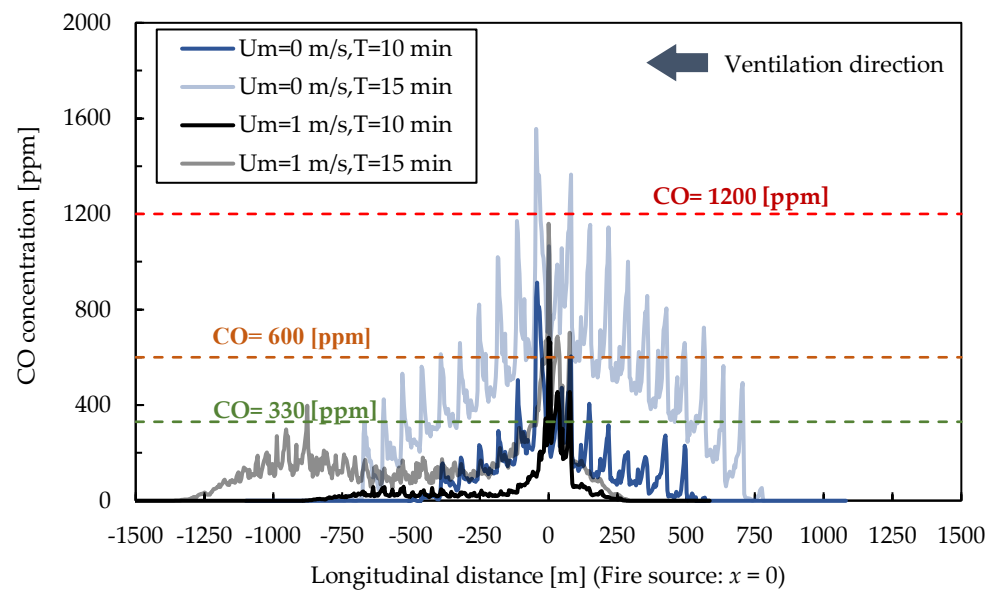


**Figure 6.** The region of descending smoke and corresponding time with  $U_m = 0$  and  $1$  m/s.

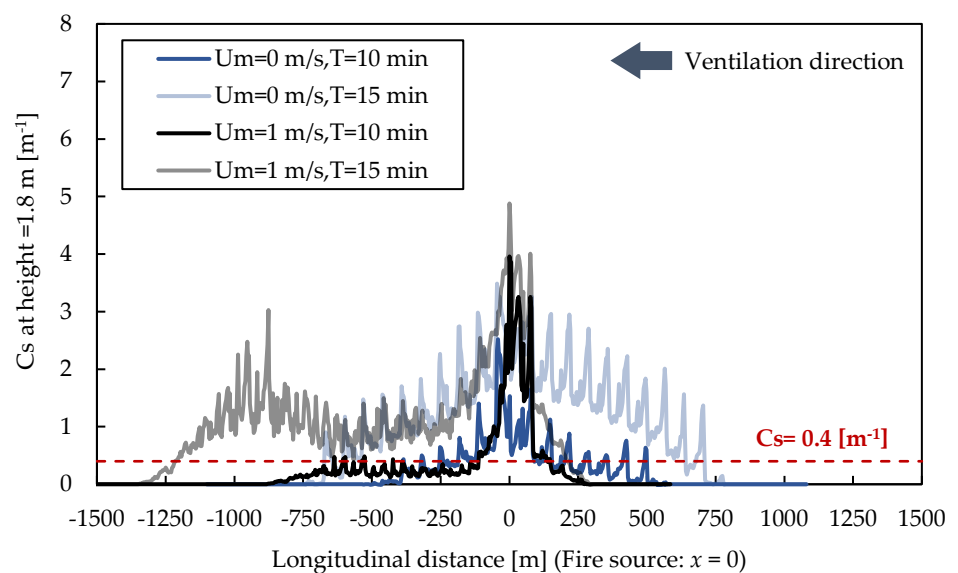
As shown in Figure 6, smoke descended on both upstream and downstream sides after 10 min when  $U_m = 0$  m/s. During the simulation time of 15 min, the region influenced by the descending smoke was around  $x = \pm 500$  m. The velocity of the horizontal propagation of descending smoke (estimated by linear regression) was around  $0.63$  m/s on the downstream side and  $0.36$  m/s on the upstream side, which was a lower velocity than evacuees' normal walking speeds of  $1.33$  m/s and  $1.27$  m/s in the tunnel (not influenced by smoke) under obstacle and obstacle-free conditions, respectively [46,58,59]. Thus, it is reasonable that the "zero-flow ventilation" strategy be adopted in Japan in keeping with the objective that tunnel users safely complete evacuation in 10 min.

When  $U_m = 1$  m/s, the region affected by descending smoke was reduced to  $x = 200$  m on the upstream side within 15 min. A safe environmental condition for self-evacuation in 10 min could also be ensured even if descending smoke existed on the upstream side. In the simulation time of 15 min, the region influenced by the descending smoke was around  $1100$  m, which was wider than the region with  $U_m = 0$  m/s.

The distribution of CO concentration and the  $C_s$  value with a longitudinal cross-section at a height of  $1.8$  m is illustrated in Figure 7. For the mode  $U_m = 0$  m/s, the CO concentration was almost under  $330$  ppm within 10 min but increased sharply in the region of  $x = \pm 500$  m within 10 to 15 min. At 15 min, the CO concentration was almost over  $600$  ppm in the region of  $x = \pm 300$  m, and the region near the fire source had even reached  $1200$  ppm, which indicated an immediate hazard to evacuees. The main reason for this rapid increase in CO concentration is considered to be that the CO generation rate is adjusted with the HRR. The HRR reaches a maximum value in  $480$  s with a quadratic fire growth rate of  $\alpha = 0.08$  kW/s<sup>2</sup>. Thus, before 8 min, the CO generation rate will not change rapidly. Moreover, when  $U_m = 0$  m/s, there is no longitudinal ventilation to dilute the CO concentration. Hence, the CO concentration in the vicinity of the fire will be relatively high. For the mode  $U_m = 1$  m/s, the CO concentration was significantly lower than  $330$  ppm for 10 min. At 15 min, the mode  $U_m = 1$  m/s maintained a relatively low CO concentration under  $330$  ppm in most regions of  $x = \pm 500$  m, but the regions of raised CO concentration extended to the downstream side of  $x = -500$ – $-1200$  m. However, it must still be noted that the above CO concentration estimation result is contingent on the CO generation rate with  $U_m = 0$  m/s being three times that of cases with longitudinal ventilation [55].



(a)



(b)

**Figure 7.** CO and  $C_s$  concentration with  $U_m = 0$  and  $1$  m/s. (a) Longitudinal CO concentration profiles at height of  $1.8$  m; (b) Longitudinal extinction coefficient  $C_s$  profiles at height of  $1.8$  m.

With respect to the  $C_s$  value, both  $U_m = 0$  and  $1$  m/s indicated that most regions were under  $C_s = 0.4$  m<sup>-1</sup> in 10 min except for the area  $x = \pm 250$  m. At 15 min, the region under  $C_s = 0.4$  m<sup>-1</sup> significantly increased ( $U_m = 0$  m/s:  $x = -650$ – $500$  m, total smoke coverage:  $1150$  m;  $U_m = 1$  m/s:  $x = -1200$ – $200$  m, total smoke coverage:  $1400$  m) for both ventilation modes. Thus, considering time and parameters (CO and  $C_s$ ) for safety evaluation finds that both  $U_m = 0$  and  $1$  m/s maintain a relatively safe environment for self-evacuation in 10 min. When further considering 15 min (assuming some evacuation delay occurs), the case of  $U_m = 1$  m/s maintained a relatively low CO concentration level compared with the case of  $U_m = 0$  m/s, but its demerit is that the region suffering smoke would expand toward the downstream side significantly. Thus, it is difficult to distinguish which ventilation mode is best when considering the hazard factors of both CO and  $C_s$  concentration for both sides in the scenario of traffic with congestion. Nevertheless, it is still observed that there are

obvious differences in the smoke environment between the simulation times of 10 min and 15 min regardless of whether  $U_m = 0$  m/s or 1 m/s.

### 3.2. Velocities 2 and 3 m/s for the Consideration of Traffic without Congestion

Figure 8 illustrates the smoke concentration ( $C_s$ ) distribution in the case of  $U_m = 2$  and 3 m/s. Longitudinal velocities of 2 and 3 m/s are usually applied in the situation of a longitudinal ventilated tunnel with no congestion traffic conditions as smoke propagation velocities are fast on the downstream side of the fire, so road tunnel users have no choice but to evacuate from the tunnel by their cars.

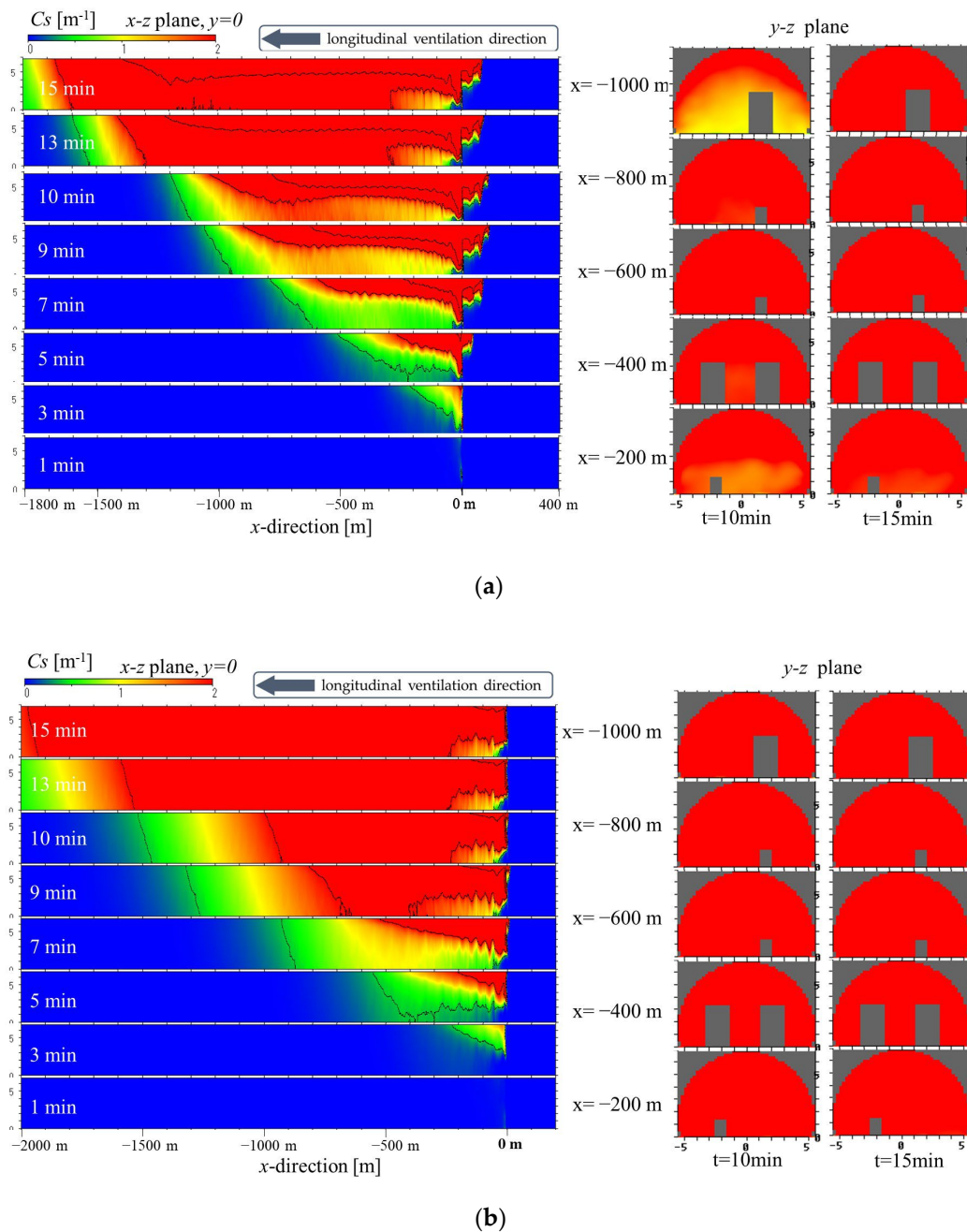


**Figure 8.** Side view of smoke distribution with  $U_m = 2$  and 3 m/s. (a) 2 m/s; (b) 3 m/s.

In  $U_m = 2$  m/s, smoke diffusion was slight on the upstream side. Back-layering length on the upstream side was confined to around  $x = 100$  m within 15 min. The first destroyed smoke stratification phenomenon was observed on the downstream side at around 5 min.

The turbulent smoke then diffused toward the road surface in the region of  $x = -200$  m and from 6 min expanded from  $x = 0$  m to  $-1800$  m in 15 min.

In  $U_m = 3$  m/s, no back-layering was observed on the upstream side. This suggests that where  $U_m = 3$  m/s is adopted in a tunnel emergency plan, the hazard of descending smoke does not need to be further discussed. On the other hand, the turbulent smoke diffused toward the tunnel road earlier for  $U_m = 3$  m/s than  $U_m = 2$  m/s. After 5 min, no smoke stratification could be observed on the downstream side. The region filled with smoke expanded to over  $x = -2000$  m in 15 min. Moreover, the smoke concentration ( $C_s$ ) distribution was heavier for 3 m/s than 2 m/s. Thus,  $U_m = 3$  m/s is good for preventing back-layering, but the downstream side's evacuation conditions are more dangerous.

A further analysis of the descending smoke regions and corresponding descending times for  $U_m = 2$  and 3 m/s is shown in Figure 9. No descending smoke influenced the environment for safe evacuation on the upstream side for both  $U_m = 2$  and 3 m/s. This indicates that a target velocity of  $U_m = 2$  m/s (lower than critical velocity) can also relatively reduce the risk of tunnel users being threatened by smoke on the upstream side due to there being no descending phenomenon. In focusing downstream of the fire source, we found that the region influenced by descending smoke increased significantly for  $U_m = 2$  and 3 m/s. The earliest smoke descending regions and corresponding times were  $x = -200$  m at 5 min for  $U_m = 2$  m/s and  $x = -300$ – $-400$  m at 5 min for  $U_m = 3$  m/s. The velocity of the horizontal propagation of descending smoke (from estimating the data in Figure 9 via linear regression) was around 2.53 m/s and 3.33 m/s for  $U_m = 2$  and 3 m/s, respectively.

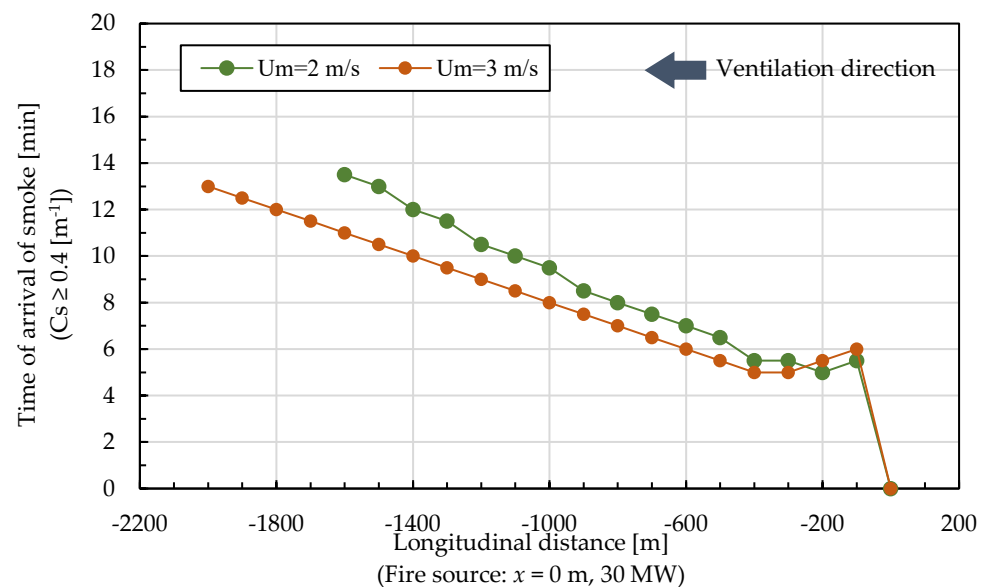
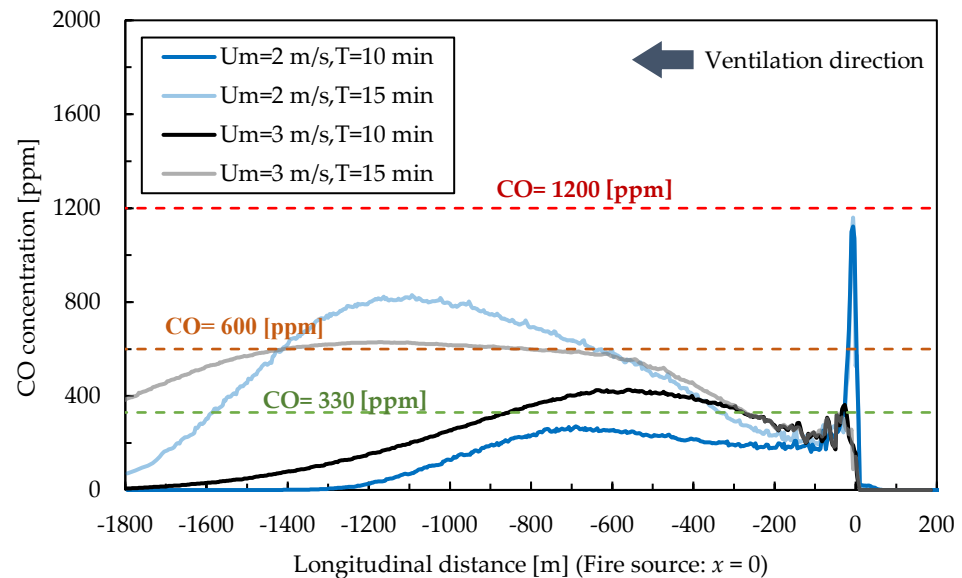


**Figure 9.** The regions of descending smoke and corresponding times with  $U_m = 2$  and 3 m/s.

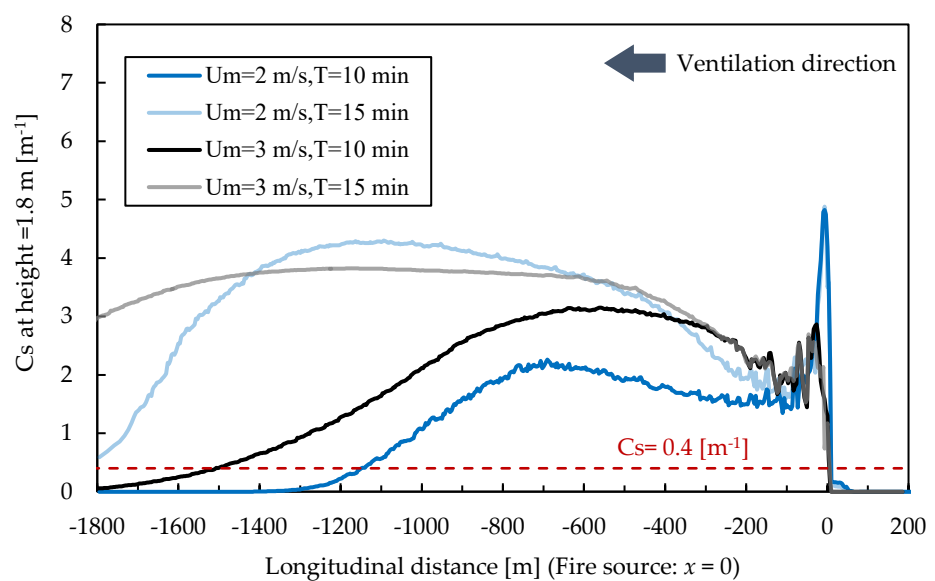
Comparing the experimental results on emergency evacuation speed in tunnels reported by Seike et al. [50], a horizontal propagation speed of 2.53 m/s is slightly faster than the mean emergency evacuation speed 2.03 m/s in non-smoke conditions. The horizontal propagation speed of 3.33 m/s is close to 3.23 m/s, which is the 97.5th percentile interval of the evacuation speed probability distribution in non-smoke conditions [50]. The comparison of the horizontal smoke propagation speed and evacuation speed indicates that although both ventilation modes  $U_m = 2$  m/s and 3 m/s were adopted based on a scenario without traffic congestion,  $U_m = 2$  m/s can be considered favorable with respect to providing a higher possibility of self-evacuation as its horizontal propagation speed is relatively close to the mean evacuation speed from the experimental results.

Figure 10 illustrates the distribution of CO concentration and  $C_s$  value in cases of  $U_m = 2$  and 3 m/s. During the 10 min evaluation time, a relatively low CO concentration

was observed when  $U_m = 2$  m/s. At 15 min, the CO concentration over 600 ppm was in the region of  $x = -600$  m to  $-1200$  m for both  $U_m = 2$  and 3 m/s. However, the CO concentration was never over 1200 ppm for  $U_m = 2$  or 3 m/s. This indicates that the risk of toxic gas decreased as the longitudinal velocity increased.



(a)



(b)

**Figure 10.** Distribution of CO and  $C_s$  concentration with  $U_m = 2$  and 3 m/s. (a) CO concentration; (b) Extinction coefficient  $C_s$ .

The  $C_s$  value distribution reveals that most regions were over the criterion of  $C_s = 0.4$  m<sup>-1</sup> for both  $U_m = 2$  and 3 m/s regardless of whether the evaluation time was 10 min or 15 min. Thus, the adoption of life safety evaluation parameters also governs the results of evaluations of evacuation safety.

Furthermore, it is interesting that the CO concentration and the  $C_s$  value were higher when  $U_m = 3$  m/s than when  $U_m = 2$  m/s in 10 min, but at 15 min, the CO concentration and the  $C_s$  value were higher when  $U_m = 2$  m/s than when  $U_m = 3$  m/s. It is noted that

more significant turbulence was observed when  $U_m = 3$  m/s than when  $U_m = 2$  m/s at 10 min, and the turbulent flow made the smoke diffusion to the road surface faster. This phenomenon is also observable in the side view of Figure 8 especially at about 600 m downstream at 9 min. As the simulation time increased, the dilution effect of longitudinal velocity on the toxic gas was more obvious; thus, when the simulation time was 15 min, both CO concentration and the  $C_s$  value were slightly lower when  $U_m = 3$  m/s.

#### 4. Influence of Longitudinal Gradients

##### 4.1. Influence of Gradients on Longitudinal Ventilation Modes 0 and 1 m/s

Figure 11 illustrates the smoke distribution for  $U_m = 0$  and 1 m/s with gradients of 0, 2, 4, and 6%. The influence of the gradients on smoke propagation was clear. For both  $U_m = 0$  and 1 m/s, the back-layering length on the upstream side increased when longitudinal gradients increased to 2% but became insensitive to gradients when longitudinal gradients increased to 4 and 6%. However, the distance of smoke propagation on the downstream side decreased significantly with the increase in the gradients for both  $U_m = 0$  and 1 m/s.

The main reason for this was that the thermal buoyancy from the chimney effect increased as the gradient increased upstream, and dynamic pressure from longitudinal ventilation was at a constant value so that the driving force from the fire plume and chimney effect would be larger than the force from the longitudinal flow, resulting in a back-layering extension on the upstream side. Meanwhile, with the gradient gradually increasing, the convection of fresh air flow was more significant and caused the more significant diffusion of the smoke layer to the road surface, meaning that the extension of the back layer became insignificant at gradients of 4 and 6%. The smoke on the downstream side was mainly affected by the relatively increasing chimney effect and was easier to move upstream, so the length of the smoke propagation downstream was reduced when the gradient increased.

Figure 12 shows the horizontal distance of the descending smoke and the corresponding times considering the factor of the gradient. The criterion of  $C_s = 0.4$  m<sup>-1</sup> at the height of 1.8 m was also selected for assessment in Figure 12. When  $U_m = 0$  m/s, the smoke stratification state without descending for at least 10 min was observed in the case of gradient 0%. However, in the case of gradients 2%, 4%, and 6%, the region of 200 m on the upstream side suffered from the hazard of descending smoke after 7.5 min, 6 min, and 5.5 min, respectively. After 15 min, the area where smoke descended to the height of 1.8 m expanded to 800 m on the upstream side. It is evident that although the smoke descending on the downstream side did not change significantly, the smoke descending on the upstream side became more rapid in tunnels with a positive inclination angle (upgrade). This also implies that earlier and faster evacuation on the upstream side is necessary when the mode  $U_m = 0$  m/s is adopted in tunnels with a gradient because descending smoke becomes faster.

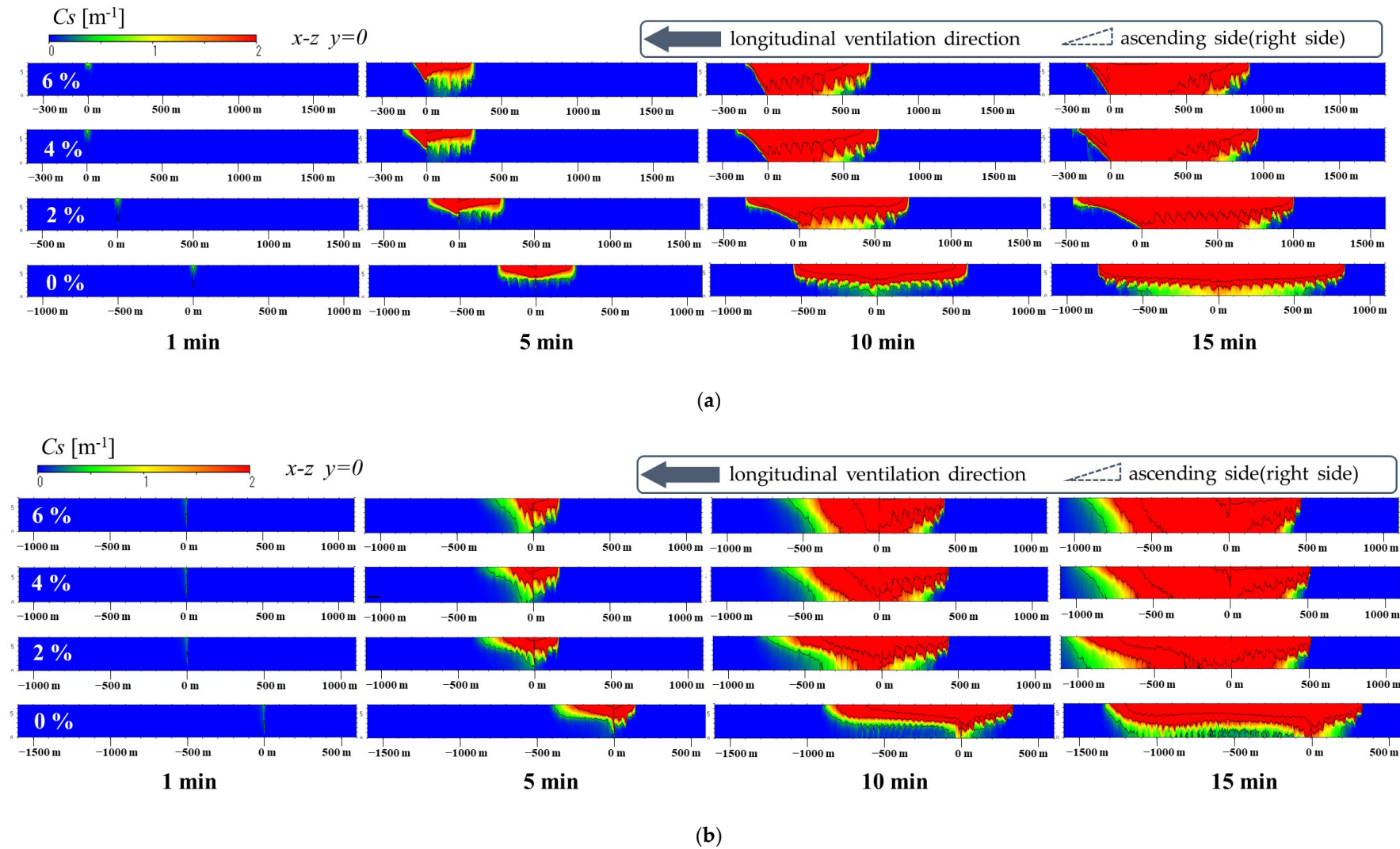
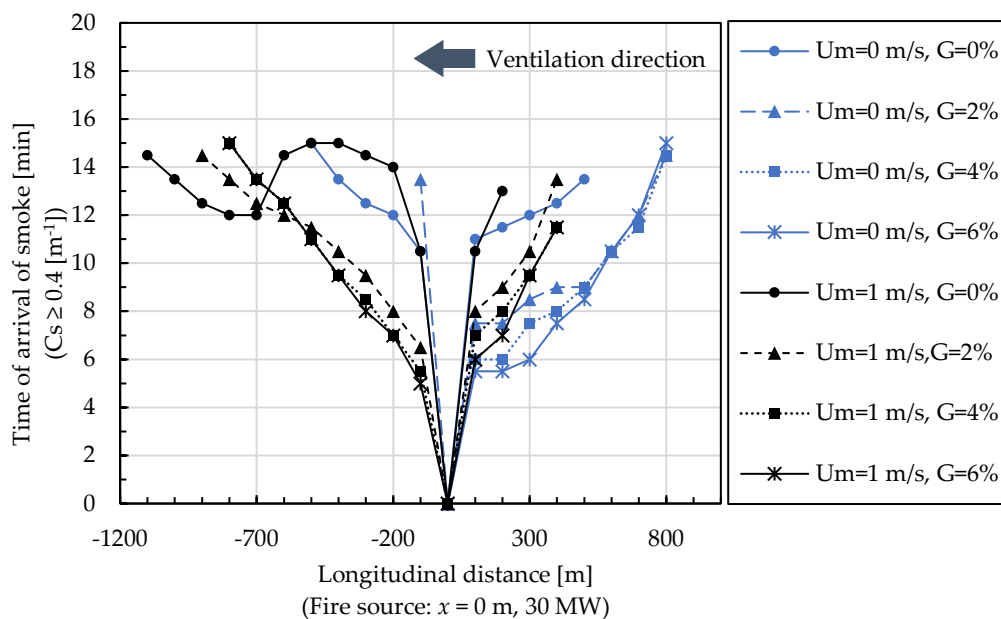


Figure 11. Side view of smoke distribution with  $U_m = 0$  and 1 m/s with gradients. (a) 0 m/s; (b) 1 m/s.



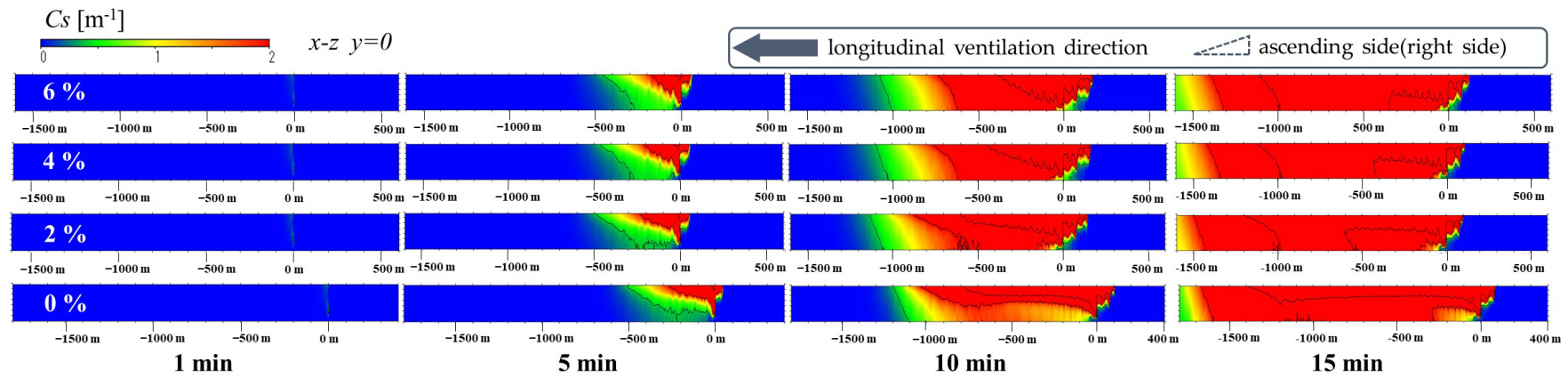
**Figure 12.** The regions of descending smoke and corresponding times with different gradients in cases of  $U_m = 0$  and  $1$  m/s.

When  $U_m = 1$  m/s, compared with the case of a 0% gradient, the area suffering the hazard of descending smoke on the downstream side decreased in the cases of gradients 2%, 4%, and 6%. The tunnel inclination increased the longitudinal component of the thermal buoyancy and resulted in smoke tending to flow to the upstream side. Despite this, the region of descending smoke was still controlled at  $x = 300$  m for 10 min because the inertial force from the longitudinal ventilation also relatively resisted the effect of the increase in the buoyancy component on the upstream. However, the destruction of smoke stratification on the downstream side occurred earlier in the cases of gradients 2%, 4%, and 6%. Earlier descending smoke was found in the region of  $x = -100$ – $-600$  m with gradients as shown in Figure 12.

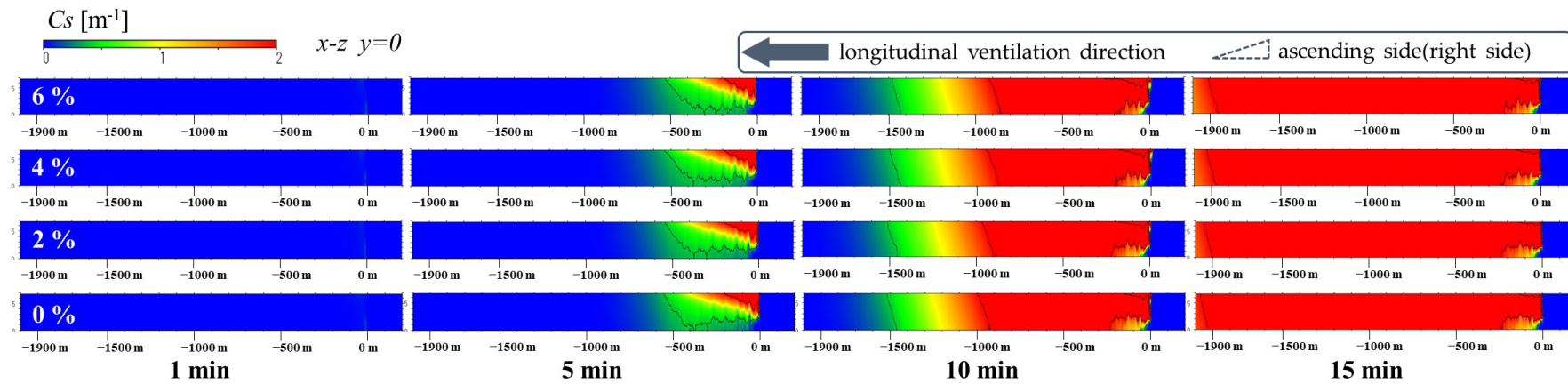
Comparing  $U_m = 0$  and  $1$  m/s in the condition of the tunnel with gradients shows that the mode  $U_m = 0$  m/s presents a relatively unfavorable evacuation environment on the upstream side since more smoke is observed to have diffused to the upstream. However, it cannot be directly assumed that low-speed ventilation ( $U_m = 1$  m/s) is better than zero-flow ventilation because Figure 12 indicates that the low-speed ventilation ( $1$  m/s) resulted in smoke descending on the downstream side earlier in the inclined tunnel.

#### 4.2. Influence of Gradients on Longitudinal Ventilation Modes 2 and 3 m/s

Figure 13 illustrates the smoke concentration ( $C_s$ ) distribution for  $U_m = 2$  and  $3$  m/s with gradients of 0%, 2%, 4%, and 6%. The back-layering was controlled at  $x = 100$  m to  $200$  m in the case of  $U_m = 2$  m/s and almost disappeared in the case of  $U_m = 3$  m/s. In addition, it is observed that the back-layering length upstream had a slight difference in the case of  $U_m = 2$  m/s with different gradients after 5 min. However, back-layering almost disappeared in the case of  $U_m = 3$  m/s even where the gradient increased. Compared with the case of the longitudinal velocity of  $2$  m/s, the smoke layer spread more widely on the downstream side when  $U_m = 3$  m/s. After 15 min, smoke diffusion reached around  $x = -2000$  m for the four gradient conditions, and the downstream side was almost filled with smoke above  $C_s 2.0$  m<sup>-1</sup>. Even though the gradient became steeper,  $U_m = 3$  m/s could satisfactorily prevent back-layering.



(a)



(b)

Figure 13. Side view of smoke distribution with  $U_m = 2$  and  $3$  m/s with gradients. (a)  $2$  m/s; (b)  $3$  m/s.

Regarding the horizontal distance of descending smoke and the corresponding times when smoke arrived as shown in Figure 14, no significant smoke descending on the upstream side was observed in the case of  $U_m = 2$  m/s. This indicates that  $U_m = 2$  m/s could also effectively prevent smoke diffusion on the upstream side even in the tunnel with a certain inclination at a fire scale of 30 MW. On the other hand, in the case of  $U_m = 2$  m/s, there was no significant difference in the region of smoke diffusion under different gradients, but the downstream smoke diffused to the road earlier as the gradient increased (see green lines in Figure 14). However, the smoke layer clearly underwent destratification when the tunnel was inclined. Thus, the descending smoke also more rapidly approached the fire source and appeared earlier on the downstream side as the gradient increased. The earliest descending smoke occurred at around  $x = -400$  m after 6 min in the case of gradient 2%; at around  $x = -100$  m after 5.5 min in the case of gradient 4%; and at around  $x = -100$  m after 5 min in the case of gradient 6%, respectively. In the case of  $U_m = 3$  m/s, the descending smoke phenomenon showed no significant difference with different gradients. This implies that the influence of the gradients on the smoke flow was negligible at the fire scale of 30 MW with a longitudinal velocity of 3 m/s. In further analyzing the horizontal propagation speed at which smoke descended to the height of 1.8 m, it was found that the propagation speed was around 3.3 m/s for the four gradient conditions, which far exceeds the average evacuation speed of people.

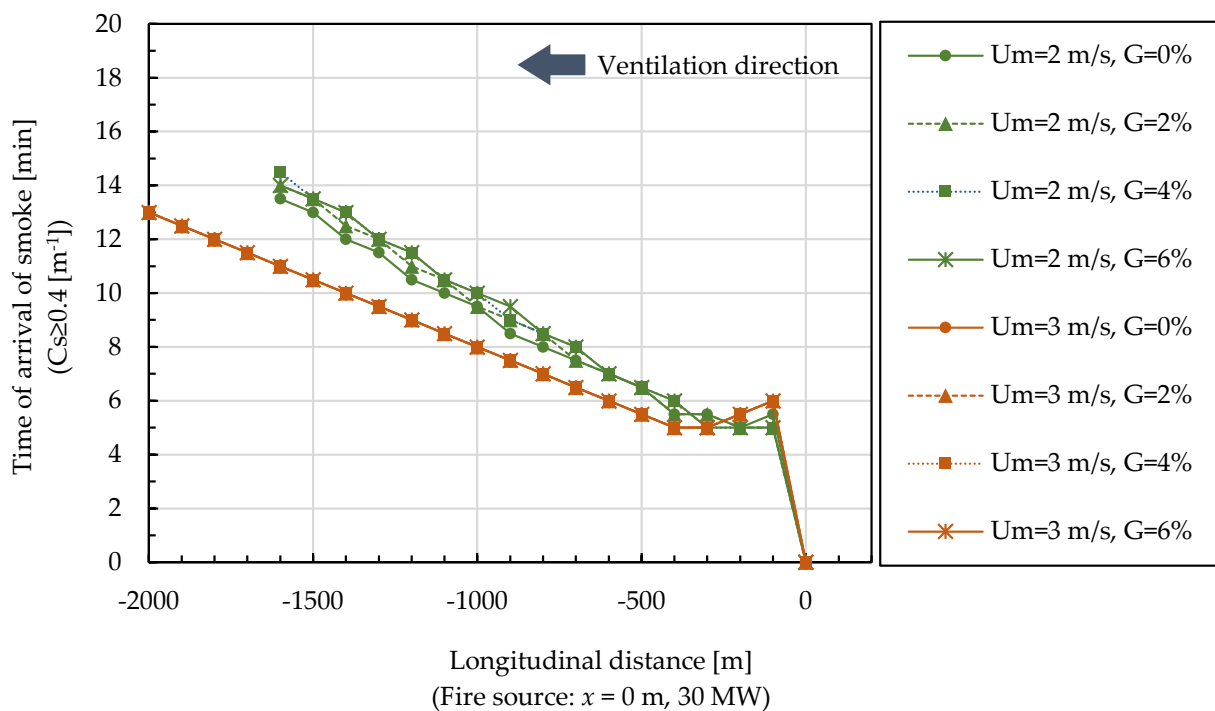


**Figure 14.** The distance of smoke spreading and corresponding times with different gradients in cases of  $U_m = 2$  and 3 m/s.

Thus, although the ventilation mode of  $U_m = 3$  m/s in the inclined tunnels (with a raised gradient) could retard downstream smoke propagation, downstream could not be considered a safe evacuation environment. The adoption of a ventilation mode close to critical velocity should be based on the premise that there is no traffic jam or evacuation to be completed on the downstream side regardless of whether the tunnel has or does not have inclination.

### **5. Discussion on Merits, Demerits, and Limitations of Longitudinal Ventilation Modes in the Unidirectional Tunnel**

Based on the discussion of the simulation results in Sections 3 and 4, the merits, de-merits, and limitations of longitudinal ventilation modes in the unidirectional tunnel are summarized in Table 8. The summarization is based on the fire scale of 30 MW and the consideration of traffic with and without congestion. Our primary finding is that it is not recommended that operations be extended to 15 min for the modes  $U_m = 0$  and 1 m/s because the deposition of smoke and the increase in CO concentration significantly worsen the upstream and downstream evacuation environment in 15 min. In addition, zero-flow ventilation and low-velocity ventilation are available for consideration with regard to traffic jam situations, but it is difficult to further distinguish which mode is more advantageous in keeping with the objective that tunnel users safely complete evacuation in 10 min, because where various hazard factors ( $C_s$  value or CO concentration) are focused, risk profiles will be found. Our other main finding with respect to inclined tunnel fires is that smoke diffused earlier on the upstream side when  $U_m = 0$  m/s, which was the opposite result of that of  $U_m = 1$  m/s; smoke diffused earlier on the downstream side when  $U_m = 1$  m/s. Although  $U_m = 2$  and 3 m/s were discussed based on a situation with no traffic congestion, the simulation results revealed that the ventilation modes of  $U_m = 2$  m/s and 3 m/s are suitable for use provided that there is not an evacuation problem downstream. Once an unexpected traffic collision or congestion occurs on the downstream side after the fire commences,  $U_m = 2$  m/s provides a higher possibility of self-evacuation on the downstream side compared with critical velocity ( $U_m = 3$  m/s) ventilation.

**Table 8.** Comparison of merits, demerits, and limitations of longitudinal ventilation modes in the unidirectional tunnel.

Ventilation Mode	Merit	Demerit	Limitation	
Traffic with congestion	0 m/s	<ul style="list-style-type: none"> <li>Can keep <math>C_s</math> and CO concentration at an acceptable safety level for 10 min for self-evacuation on both the upstream and downstream sides (limited to the horizontal tunnel).</li> </ul>	<ul style="list-style-type: none"> <li>When the evacuation process is over 10 min, hazard of increasing CO concentration arises.</li> <li>When tunnel has increasing gradient, the ascending side does not favor evacuation as smoke diffused earlier than no gradient cases.</li> </ul>	<ul style="list-style-type: none"> <li>Not recommended that tunnel emergency response with these two ventilation modes is extended to more than 10 min or to 15 min.</li> <li>Difficult to directly distinguish which ventilation mode (0 and 1 m/s) is relatively superior in the scenario of traffic with congestion when considering both the <math>C_s</math> value and CO concentration.</li> <li>Whether these two modes are available for large-scale fires is unclear.</li> </ul>
	1 m/s	<ul style="list-style-type: none"> <li><math>U_m = 0</math> m/s's merit.</li> <li>When considering 15 min evacuation time, <math>U_m = 1</math> m/s would maintain a relatively low CO concentration level compared with the case of <math>U_m = 0</math> m/s.</li> </ul>	<ul style="list-style-type: none"> <li>When focusing on the <math>C_s</math> value, this mode reveals a relatively unfavorable evacuation environment on the downstream side compared with <math>U_m = 0</math> m/s.</li> <li>When tunnel has increasing gradient, the descending side (left side) does not favor evacuation as the smoke diffused earlier from the fire source.</li> </ul>	
Traffic without congestion	2 m/s	<ul style="list-style-type: none"> <li>Can prevent the risk of tunnel users being threatened by smoke on the upstream side.</li> <li>Provides higher possibility of self-evacuation than critical velocity ventilation once an unexpected traffic collision or congestion occurs on the downstream side after the fire begins.</li> </ul>	<ul style="list-style-type: none"> <li>When tunnel has increasing gradient, the descending smoke downstream of the fire source would be much closer to the fire source and occur earlier.</li> </ul>	<ul style="list-style-type: none"> <li>It is unclear whether this mode is still available for the scenario of traffic without congestion once the fire scale increases.</li> </ul>
	3 m/s	<ul style="list-style-type: none"> <li>Smoke distribution would not be significantly influenced by changes to gradients.</li> </ul>	<ul style="list-style-type: none"> <li>Does not favor evacuation on the downstream side regardless of whether tunnel is with or without gradients.</li> </ul>	<ul style="list-style-type: none"> <li>Should only be adopted on the basis that there cannot be traffic congestion or an evacuation delay on the downstream side.</li> </ul>

Note: This table is based on the condition of having a fire scale of 30 MW, and the CO concentration estimation is based on the condition that the CO generation rate with  $U_m = 0$  m/s is three times that of cases with longitudinal ventilation.

## 6. Conclusions

This study was motivated by the demand for understanding the various longitudinal ventilation modes and the premises and consequences of such modes when adopted. Considering scenarios of traffic with and without congestion, this study compared ventilation modes in two pairs based on the same fire scale of 30 MW with four longitudinal gradients (0%, 2%, 4%, 6%). The analysis focused on the self-evacuation phase. The main findings of this study are as follows:

- According to the simulation results, both  $U_m = 0$  and  $U_m = 1$  m/s are conducive to maintaining the stratification of smoke and ensuring the safety of the environment for 10 min (self-evacuation phase) in traffic with congestion, as the  $C_s$  value and CO concentration in most areas were below the  $0.4 \text{ m}^{-1}$  and IDHL values (1200 ppm), respectively, at a 1.8 m height level. However, it is not recommended that the tunnel emergency response be extended to more than 10 min or to 15 min with either ventilation mode because the diffusion of smoke and the increase in CO concentration significantly worsened the upstream and downstream evacuation environments. Thus, the tunnel emergency response should be completed in 10 min when there is traffic congestion.
- Considering the  $C_s$  value (for the horizontal tunnel),  $U_m = 1$  m/s revealed a relatively unfavorable evacuation environment on the downstream side compared with  $U_m = 0$  m/s in 10 min. However, in view of CO concentration, an unfavorable evacuation environment was significant at 15 min where  $U_m = 0$  m/s was compared with  $U_m = 1$  m/s. In further discussion of inclined tunnels, descending smoke became serious on the upstream side in the case of  $U_m = 0$  m/s and became serious on the downstream side in the case of  $U_m = 1$  m/s. It is difficult to distinguish which ventilation mode (0 or 1 m/s) has relatively superior performance when considering both hazard factors CO and  $C_s$  on both sides. However, it should be noted that the result of the CO concentration estimation in this study was based on the assumption that the CO generation rate when  $U_m = 0$  m/s is three times that of cases with longitudinal ventilation.
- The comparison of  $U_m = 2$  and 3 m/s based on traffic conditions without congestion revealed that a target velocity of  $U_m = 2$  m/s (lower than critical velocity) can also prevent the risk of tunnel users being threatened by smoke on the upstream side since no descending phenomenon was observed. Both modes were deemed available for implementation provided that no traffic jam could occur downstream. The relatively slow propagation of descending smoke in the case of  $U_m = 2$  m/s increased the possibility of a successful evacuation if a second traffic incident were to occur downstream of the fire source.

This study explored the verification of turbulence re-productibility and chose a finer grid size to simulate the results of various longitudinal ventilation modes in various gradients tunnels. The above findings contribute to a more objective evaluation of the difference between various longitudinal ventilation modes considering traffic conditions and provide more useful insights for the emergency planning of longitudinal ventilation operation in tunnel fires. Additionally, the influence of far larger-scale fires on the evacuation environment under different longitudinal ventilation modes has not yet been studied, and it remains a future task to analyze these longitudinal ventilation modes in combining evacuation models for a complete quantitative risk analysis (QRA).

**Author Contributions:** Conceptualization, P.-W.T., H.-C.C. and N.K.; methodology, P.-W.T., H.-C.C. and N.K.; validation, P.-W.T., H.-C.C. and N.K.; formal analysis, P.-W.T., H.-C.C. and N.K.; investigation, P.-W.T., H.-C.C. and N.K.; resources, N.K.; data curation, P.-W.T. and H.-C.C.; writing—original draft preparation, P.-W.T., H.-C.C. and N.K.; writing—review and editing, N.K., M.S., M.H., S.-W.C. and T.-S.S.; visualization, P.-W.T., H.-C.C. and N.K.; supervision, N.K., M.S., M.H., S.-W.C. and T.-S.S.; project administration, N.K., M.S., M.H., S.-W.C. and T.-S.S.; funding acquisition, N.K., M.S., M.H., S.-W.C. and T.-S.S. All authors have read and agreed to the published version of the manuscript.

**Funding:** Grants from the Ministry of Education, Culture, Sports, Science and Technology, Japan in aid of scientific research (number: 20K05008).

**Data Availability Statement:** Not applicable.

**Acknowledgments:** The authors are sincerely grateful for the funding aid from the Ministry of Education, Culture, Sports, Science and Technology, Japan.

**Conflicts of Interest:** The authors declare no conflict of interest.

## Appendix A

Fundamental governing equations, discretization schemes, and boundary conditions

In the present study, we executed our self-developed 3D CFD code (Kawabata et al., 1998) using LES as the turbulence model (Smagorinsky model). As the governing equations of the heat and air flows in the tunnel, we used the continuity equation, the momentum equation, the equation of energy conservation, the equation of state, and the equation of smoke concentration. The LES turbulence model was applied only to the velocity field, whereas the zero-equation model was applied to both the temperature and density fields. As the pressure differences were around 0.1% of the barometric pressure, we assumed that the density change depended on temperature alone.

The thermal convection current is influenced by the gas volume expansion that accompanies the large temperature rise. Therefore, it must be treated as a compressible fluid in the simulation. Additionally, we assumed that the temperature fluctuations  $T'$  of the smaller grid scale in the temperature field  $T$  (K) of the LES turbulence model were smaller than the velocity fluctuations  $v'$  in the velocity field  $\mathbf{v}$  (m/s):

The governing equations were thus given as follows:

Continuity equation

$$\frac{\partial \rho}{\partial t} + \nabla(\rho \mathbf{v}) = 0 \quad (\text{A1})$$

Momentum equation (Navier-Stokes equation)

$$\rho \frac{D\mathbf{v}}{Dt} = -\nabla P + \nabla \tau + \rho \mathbf{g} + \rho \mathbf{v} \nabla \mathbf{v} + F \quad (\text{A2})$$

where

$$\frac{D}{Dt} = \frac{\partial}{\partial t} + (\mathbf{v} \cdot \nabla), \quad \tau = (\mu_m + \mu_t)[(\nabla \cdot \mathbf{v}) + (\nabla \cdot \mathbf{v})^T - \frac{2}{3} \nabla \mathbf{v}] \quad (\text{A3})$$

Here  $\rho$  is the density [ $\text{kg}/\text{m}^3$ ].  $t$  is the time from ignition [s],  $\mathbf{v}$  means the velocity vector of air [m/s].  $\mathbf{g}$  is the gravitational vector, determined by the tunnel gradient.  $\tau$  is stress tensor.  $\mu_m$  is the molecular viscosity coefficient.  $\mu_t$  is the turbulent (eddy) viscosity coefficient based on the by the LES model. Since the paper focuses on a full-scale tunnel, the internal flow is considered turbulent. Therefore, it is assumed that  $\mu_m \ll \mu_t$ , and  $\mu_m$  can be ignored.  $F = \left(0, \frac{\rho v_x^2}{R}, 0\right)$  is the centrifugal force (vector component) due to the radius of curvature  $R$  of the  $x$ -axis, which applies only to the equation of motion in the  $y$ -direction. Since there is no bend in this paper,  $1/R$  is assumed as 0 in the Equation (A2).

Energy equation

$$\rho \frac{DC_v T}{Dt} = \nabla \left( \left( k + \frac{C_v \mu_t}{Pr_t} \right) \nabla T \right) + Q_h - P(\nabla \mathbf{v}) \quad (\text{A4})$$

Here  $T$  is the temperature ( $T = \Delta T$  (temperature difference) +  $T_0$  (absolute temperature)) [K].  $C_v$  is the specific heat at constant volume.  $k$  is thermal conductivity coefficient. The quantities  $Pr_t$  is the turbulent Prandtl number.  $Q_h$  is the Heat release rate (HRR) [ $\text{W}/\text{m}^3$ ]. We assumed the internal flow in the tunnel is the turbulent flow the same as the assumption in the viscosity coefficient and neglected the thermal conductivity coefficient  $k$  in the Equation (A4) in the present study.

Equation of state

$$\rho = \frac{P}{RT} \quad (\text{A5})$$

Here  $R$  is the gas constant. The density  $\rho$  is affected by smoke particles and CO concentration, but in the case of a tunnel fire, the smoke mass concentration is around several  $\text{g}/\text{m}^3$ , and the CO concentration is around several thousand ppm, so the effect on air density is less than 1%. Therefore, the density of flow was considered as air alone.

Based on these assumptions, the diffusion equation of smoke particles is as follows.

Equation of smoke concentration

$$\frac{DM}{Dt} = \nabla \left( \frac{\mu_t}{\rho \sigma_{ct}} \nabla M \right) + S_c \quad (\text{A6})$$

$M$  is the mass concentration of smoke [ $\text{g}/\text{m}^3$ ],  $S_c$  is the smoke generation rate (SGR) [ $\text{g}/(\text{s} \cdot \text{m}^3)$ ] per unit volume.  $\sigma_{ct}$  is the Turbulent Schmidt number.

The turbulent (eddy) viscosity coefficient  $\mu_t$  was computed as follows:

$$\mu_t = \rho (C_{sgs} \Delta)^2 \left[ \frac{1}{2} \left( \frac{\partial v_i}{\partial x_j} + \frac{\partial v_j}{\partial x_i} \right)^2 - \frac{2}{3} (\nabla \mathbf{v})^2 \right]^{\frac{1}{2}} \quad (\text{A7})$$

Here  $C_{sgs}$  is the Smagorinsky Constant,  $\Delta$  is the size of the filter and is given by  $(dx dy dz)^{1/3}$ . The subscript  $i$  and  $j$  mean the directional components along the  $x$ ,  $y$ , and  $z$  axes.

The  $P$  means the pressure in the tunnel fire. It depends on static pressure at zero flow (absolute pressure  $P_0$ ) and the differential pressure distribution  $p$  as follows:

$$P = P_0 + p \quad (\text{A8})$$

Here  $P_0$  is of the order of  $10^5$  [Pa],  $p$  is approximately the order of 10 [Pa]. Hence,  $p$  is smaller than  $1/1000 P_0$ ; therefore, the equation of state (Equation (A5)) can be rewritten as:

$$\rho \approx \frac{P_0}{RT} \quad (\text{A9})$$

The change in the density ( $\rho$ ) is mainly govern by the change in temperature field. We hence obtain the following relationship:

$$\frac{1}{\rho} \frac{D\rho}{Dt} = - \frac{1}{T} \frac{DT}{Dt} \quad (\text{A10})$$

Substituting Equation (A10) into the continuity Equation (A1), and then applying Equation (A4), we can obtain the following equation.

$$\nabla \mathbf{v} = \frac{1}{C_p \rho T} \left[ \nabla \left( C_v \frac{\mu_t}{P_{rt}} \nabla T \right) + Q_h \right] \quad (\text{A11})$$

The momentum Equation (A2) can be expressed as a function of  $p$ :

$$\frac{D\mathbf{v}}{Dt} = - \frac{1}{\rho} \nabla p + \frac{1}{\rho} \nabla \tau + \frac{\rho - \rho_0}{\rho} \mathbf{g} \quad (\text{A12})$$

where  $\rho_0$  is the density during normal periods ( $T = T_0$ ,  $P = P_0 + p$ ), the third term on the right-hand side of Equation (A12) is a buoyancy term. Substituting the buoyancy term into

Equation (A9), we can obtain the following equation by omitting the  $P_0/P$  and  $p/P$  of the low Mach number approximation.

$$\frac{\rho - \rho_0}{\rho} \mathbf{g} = \left(1 - \frac{T}{T_0}\right) \mathbf{g} \quad (\text{A13})$$

Hence, the governing equations in the present study are the continuity Equation (A11), the momentum Equation (A12), the equation of energy (A4), the equation of state (A9), the equation of smoke concentration (A6), and the turbulence model (A7).

The heat released by the fire was limited to the region above the fire source (analogous to a large electric heater in the region), and the combustion reactions were omitted. In actual fires, much of the radiation heat is absorbed by the copious volumes of murky smoke. Therefore, the influence of radiation heat in the tunnel fire was not involved in the present numerical analysis of flow field.

The time-advancing in the present numerical simulation is calculated by the explicit Crank–Nicolson method.

The time-advancing procedure ( $t^n \rightarrow t^{n+1}$ ) based on SMAC method can explain as follows.

Firstly, expressing momentum equation (Navier–Stokes equation) as

$$\rho \frac{D\mathbf{v}}{Dt} = -\nabla P + f(\mathbf{v})$$

- (1) Compute the predicted value  $\tilde{\mathbf{v}}$  when  $t^{n+1}$  by the predictor of Euler explicit method.

$$\frac{\tilde{\mathbf{v}} - \mathbf{v}^n}{\Delta t} = -\frac{1}{\rho^n} \nabla p^n + f(\mathbf{v}^n)$$

Here  $\mathbf{v}^n$ ,  $\rho^n$ ,  $p^n$  means the velocity vector, density, and pressure when time step is  $t^n$ .

- (2) Compute the another predicted value (temperature, mass concentration)  $\tilde{T}$ ,  $\tilde{M}$  when  $t^{n+1}$  by the Euler explicit method too.  
 (3) Calculate  $T^{n+1}$ ,  $M^{n+1}$  when time step of  $t^{n+1}$  using the predicted value, and then calculate the density  $\rho^{n+1}$  from the equation of state (A5).  
 (4) Calculate velocity prediction value  $\tilde{\mathbf{v}}$  by the corrector of Euler semi-implicit method.

$$\frac{\tilde{\mathbf{v}} - \mathbf{v}^n}{\Delta t} = -\frac{1}{\rho^{n+1}} \nabla p^n + f(\tilde{\mathbf{v}}) \quad (\text{A14})$$

- (5) Express the formula with pressure as  $p^{n+1}$

$$\frac{\mathbf{v}^{n+1} - \mathbf{v}^n}{\Delta t} = -\frac{1}{\rho^{n+1}} \nabla p^{n+1} + f(\tilde{\mathbf{v}}) \quad (\text{A15})$$

And then, from the difference between Equations (A14) and (A15), the pressure difference  $\Phi = p^{n+1} - p^n$  in time difference  $\Delta t$  can express as.

$$t \nabla \frac{1}{\rho^{n+1}} \nabla \Phi = \nabla \tilde{\mathbf{v}} - \nabla \mathbf{v}^{n+1} \quad (\text{A16})$$

Here, the Equation (A11) is substituted into  $\nabla \mathbf{v}^{n+1}$  to solve the above Equation (A16) and calculate  $\Phi$ .

- (6) And then the pressure and velocity when time step is  $t^{n+1}$  can be calculated through following equation.

$$p^{n+1} = p^n + \Phi \quad (\text{A17})$$

$$\mathbf{v}^{n+1} = \tilde{\mathbf{v}} + \frac{\Delta t}{\rho} \nabla \Phi \quad (\text{A18})$$

Boundary conditions of velocity and temperature field on the wall surface used in Fireless are explained as follows.

First, for the velocity field, we consider cell center in contact with the wall and divided into three cases.

- (i) Laminar boundary layer.
- (ii) The wall function (Prandtl's law of wall) for a smooth wall involving in the turbulent boundary layer.
- (iii) The same as the surface roughness.

In the case of (i), since the flow on the sticky bottom layer (closest to the wall) is close to laminar layer, the velocity distribution  $u_i$  is assume as

$$\frac{u_i}{u_\tau} = \frac{u_\tau \delta}{\nu} \quad (\text{A19})$$

Here, the friction velocity  $u_\tau$  is defined as  $u_\tau = \sqrt{\tau_w/\rho}$ ,  $\delta$  is the distance between the cell center and the wall,  $\nu$  and  $\rho$  are the kinematic viscosity and density of air, respectively.

And then the frictional stress ( $\tau_w$ ) can be calculated by substituting in Equation (A19) as follows.

$$\tau_w = \mu u_i / \delta \quad (\text{A20})$$

In the case of (ii), the velocity distribution  $u_i$  is calculated by the following formula, following the wall law of a smooth wall.

$$\frac{u_i}{u_\tau} = \frac{1}{0.4} \ln \frac{\delta u_\tau}{\nu} + 4.1 \quad (\text{A21})$$

Here,  $u_\tau = \sqrt{\tau_w/\rho}$ .

In the case of (iii), it is assumed that the wall roughness  $\varepsilon$  is almost the same as  $\delta$ , logarithmic law for the hydrodynamically rough wall is applied, and the velocity distribution  $u_i$  is obtained by the following equation.

$$\frac{u_i}{u_\tau} = 5.75 \log \frac{\delta}{\varepsilon} + 8.5 \quad (\text{A22})$$

Secondly, the heat flux  $q_w$  of the thermal flume absorbed by the wall depends on the heat-transfer coefficient  $h_w$ :

$$q_w = h_w(T_\infty - T_w) \quad (\text{A23})$$

Here  $T_w$  and  $T_\infty$  are the temperatures at the wall surface and outside the temperature boundary layer, respectively. The latter was determined as the temperature at the center of the cell adjacent to the wall.

The heat transfer coefficient is not a physical property value unique to the fluid, but changes in a complex manner depending on the type of fluid, flow conditions, object shape, surface roughness, etc. Many empirical equations of the heat transfer coefficient have been proposed so far to show the relationship between the Bulk flow and the heat transfer coefficient in a circular tube or a flat plate, and the cells in contact with each other. It takes some ingenuity to find the relationship between center of the cell adjacent to the wall.

In the Fireless, three heat transfer conditions can be selected.

- (i)  $h_w$  is a constant.
- (ii)  $h_w$  is given by the formula of [43]

$$h_w = 5.92 + 3.95(u_i)/T_i \quad (\text{A24})$$

Here  $u_i$  is the velocity component in the center of the cell adjacent to the wall. It can be obtained from boundary conditions of velocity.  $T_i$  is the temperature of the center of the cell adjacent to the wall which dividing by 293 [K].

The Jürges's model is originally a relational formula between the velocity, the temperature, and the heat transfer coefficient outside the temperature boundary layer. Since the cell size in the case of full-scale tunnel simulation is around 0.2 m, which is the same as the thickness degree of the temperature boundary layer. It is considered applicable. However, since the grid size is usually set up at around 1 cm in a reduced model tunnel, the Jürges's model cannot be applied as it is.

(iii)  $h_w$  converting by Colburn's analogy

$$\frac{h_w}{C_p} \cdot \frac{u_c}{\tau_w} = \alpha P_r^{-\frac{2}{3}} \quad (\text{A25})$$

where  $P_r$  is Prandtl number [-],  $\tau_w$  is friction stress [ $\text{kg}/\text{m} \cdot \text{s}^2$ ] of the wall,  $\rho$  is the flow density [ $\text{kg}/\text{m}^3$ ],  $u_c$  is velocity of the flow [ $\text{m}/\text{s}$ ],  $C_p$  is the specific heats at constant pressure,  $\alpha$  is a constant 1.6 which can be artificially adjusted in simulator.

Colburn's analogy is an empirical formula can describe the relation between the ratio of heat transfer coefficient and heat flow, and the ratio of the momentum flow and frictional stress in the Bulk flow outside the temperature boundary layer. This analogy method is intended for the describing temperature boundary layer in case of a reduced model by considering the heat flow and momentum flow in the cell close to the wall surface rather than in the Bulk flow. Based on the above heat transfer conditions explanation, Jürges's model was used in the present study because it is best agreeing with past full-scale experimental results.

For the heat conduction in the tunnel wall, a one-dimensional heat conduction equation is solved that considers only the heat conduction in the wall thickness direction. However, if the grid size of the wall where in contact with the inner side of the tunnel wall is too large, the amount of heat absorption would increase and results in the temperature of the wall surface be underestimated. Therefore, it is desirable to set the ratio of the heat capacity between the grid size which contact with the wall and the grid size on the wall surface as small as possible. Kawabata et al., (2003) [39] reported that the division size where closest to the inside of the wall suitably set at the order of around 1mm for thermal conductivity reproducing. In the present study, the thickness of the wall is 175 mm and divided into nine divisions increasing at a ratio of 1.6 times as it goes to the outer surface of the wall (the division is unequal). The division size where closest to the inside of the wall is 2.33 mm. Despite this, the order of division size is still close to the previous study of 1mm. The material is concrete (specific heat [ $\text{J}/(\text{kg} \cdot \text{K})$ ], density 2100 [ $\text{kg}/\text{m}^3$ ], thermal conductivity 1.10569 [ $\text{W}/\text{m} \cdot \text{K}$ ]).

Since the curved boundaries (curved wall) are established by stacked rectangle grids in Fireles, it does not follow the arc-shaped ceiling smoothly but becomes stepped. Therefore, the surface area increases compared to the circular shape, and the frictional resistance and the heat absorption amount are expected to be large, so it is necessary to correct the friction resistance and the heat absorption amount. In Fireles, we use the diagonal line ( $l = \sqrt{\Delta y^2 + \Delta z^2}$ ) of grids ( $\Delta y, \Delta z$ ) to convert heat absorption amount acting on the diagonal line as following figure.

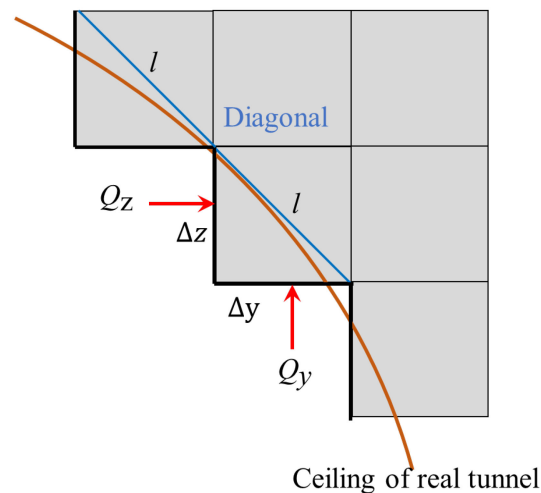


**Figure A1.** Diagram of frictional resistance and the heat absorption amount adjusting for curved boundaries.

The effective heat absorption amount in  $xy$ -surface of the grid adjusted by equation  $Q_y \Delta y l / (\Delta y + \Delta z)$ . The heat absorption amount in  $xz$ -surface of the grid adjusted by equation  $Q_z \Delta z l / (\Delta y + \Delta z)$ . Here  $Q_y$  and  $Q_z$  mean the heat absorption amount in the  $xy$ -surface and  $xz$ -surface of the grid calculating in the simulation. Moreover, friction stress is also converted to stress acting on the diagonal line by multiplying the coefficient in the same way.

## References

- Huang, T. Safety Assessment of Longitudinal Ventilation System and Point Extraction Ventilation System in Road Tunnel Fire. Ph.D. Thesis, Graduate School of Natural Science & Technology Kanazawa University, Kanazawa, Japan, 2021. Available online: <http://hdl.handle.net/2297/0062850> (accessed on 9 June 2021).
- Huang, T.; Kawabata, N.; Seike, M.; Hasegawa, M.; Chien, S.W.; Shen, T.S. Comparison of Fire Safety Evaluation between Longitudinal Ventilation System and Concentrated Smoke Exhaust System for Road Tunnels. *J. Jpn. Soc. Civ. Eng. Ser. F2* **2021**, *77*, 41–59. (In Japanese) [[CrossRef](#)]
- Yamada, M. Transition of Japanese Road Tunnel Ventilation System and Future Issues. Ph.D. Thesis, Graduate School of Natural Science & Technology, Kanazawa University, Kanazawa, Japan, 2015. Available online: <http://hdl.handle.net/2297/42269> (accessed on 14 February 2021).
- Kohl, B.; Senekowitsch, O.; Nakahori, I.; Sakaguchi, T.; Vardy, A.E. Risk Assessment of Fire Emergency Ventilation Modes during Traffic Congestion in Unidirectional Tunnels with Longitudinal Ventilation. In Proceedings of the 17th ISAVFT, BHR group, Lyon, France, 13 September 2017.
- World Road Association (PIARC). *Road Tunnels: Operational Strategies for Emergency Ventilation (No. 2011R02)*; PIARC: La Défense, France, 2011; pp. 41–63.
- Nakahori, I.; Sakaguchi, T.; Kohl, B.; Forster, C.; Vardy, A. Risk assessment of zero-flow ventilation strategy for fires in bidirectional tunnels with longitudinal ventilation. In Proceedings of the 16th International Symposium on Aerodynamics, Ventilation and Fire in Tunnels, Seattle, WA, USA, 15 September 2015; pp. 15–17.
- Ho, Y.T.; Kawabata, N.; Seike, M.; Hasegawa, M.; Chien, S.W.; Shen, T.S. Scale Model Experiments and Simulations to Investigate the Effect of Vehicular Blockage on back-layering Length in Tunnel Fire. *Buildings* **2022**, *12*, 1006. [[CrossRef](#)]
- Sturm, P.; Beyer, M.; Rafiei, M. On the problem of ventilation control in case of a tunnel fire event. *Case Stud. Fire Saf.* **2017**, *7*, 36–43. [[CrossRef](#)]
- Hsu, W.S.; Huang, Y.H.; Shen, T.Z.; Cheng, C.Y.; Chen, T.Y. Analysis of the Hsuehshan Tunnel Fire in Taiwan. *Tunn. Undergr. Space Technol.* **2017**, *69*, 108–115. [[CrossRef](#)]
- Kunikane, Y.; Kawabata, N.; Ishikawa, T.; Takekuni, K.; Shimoda, A. Thermal Fumes and Smoke Induced by Bus Fire Accident in Large Cross Sectional Tunnel. In Proceedings of the 5th JSME-KSME Fluids Engineering Conference, Nagoya, Japan, 17–21 November 2002; pp. 17–21.
- Kunikane, Y.; Kawabata, N.; Okubo, K.; Shimoda, A. Behaviour of Fire Plume in a Large Cross Sectional Tunnel. In Proceedings of 11th International Symposium on AVVT, Luzern, Switzerland, July 2003; pp. 78–93.

12. Ingason, H.; Li, Y.Z.; Lönnemark, A. *Tunnel Fire Dynamics*, 1st ed.; Springer: New York, NY, USA, 2014; pp. 153–156. ISBN 978-1-4939-2198-0.
13. The European Parliament and the Council of the European Union. *Directive 2004/54/EC on Minimum Safety Requirements for Tunnels in the Trans-European Road Network*; European Parliament: Strasbourg, France, 2004.
14. Ingason, H. Design Fire Curves for Tunnels. *Fire Saf. J.* **2009**, *44*, 259–265. [[CrossRef](#)]
15. Kohl, B.; Botschek, K.; Hörhan, R. Austrian Risk Analysis for Road Tunnels. In Proceedings of the 3rd International Conference, Tunnel Safety and Ventilation, Graz, Austria, 15–17 May 2006.
16. Kohl, B.; Forster, C. Risk Analysis as Decision making Tool for Tunnel Design and Operation. In Proceedings of the 6th International Conference ‘Tunnel Safety and Ventilation’, Graz, Austria, 23–25 April 2012; pp. 17–25.
17. Yamazaki, T.; Yokota, M.; Kawabata, N. Study on the Potential Risks Analysis Approach for Tunnel Fires in Expressway Tunnels. *J. Jpn. Soc. Civ. Eng. Ser. F2* **2015**, *71*, 31–46. (In Japanese) [[CrossRef](#)]
18. Qi, D.; Yang, S.; Shu, C. An exploratory study on road tunnel with semi-transparent photovoltaic canopy—From energy saving and fire safety perspectives. *Build. Simul.* **2022**, *15*, 537–548. [[CrossRef](#)]
19. Ji, J.; Wan, H.; Li, J.; Sun, J. A numerical study on upstream maximum temperature in inclined urban road tunnel fires. *Int. J. Heat Mass Transf.* **2015**, *88*, 516–526. [[CrossRef](#)]
20. Ingason, H. *Handbook of Tunnel Fire Safety*, 2nd ed.; ICE Publishing: London, UK, 2012; pp. 273–308.
21. Chen, F.; Chien, S.W.; Jang, H.M.; Chang, W.J. Stack effects on smoke propagation in subway stations. *Continuum Mech.* **2003**, *15*, 425–440. [[CrossRef](#)]
22. Zhang, X.; Zhang, Z.; Tao, H. A numerical study on critical velocity and back-layering length with train’s blockage in longitudinally ventilated tunnel fires. *Tunn. Undergr. Space Technol.* **2021**, *116*, 104093. [[CrossRef](#)]
23. Caliendo, C.; Ciambelli, P.; de Guglielmo, M.L.; Meo, M.G.; Russo, P. Numerical simulation of different HGV fire scenarios in curved bi-directional road tunnels and safety evaluation. *Tunn. Undergr. Space Technol.* **2012**, *31*, 33–50. [[CrossRef](#)]
24. Caliendo, C.; Ciambelli, P.; de Guglielmo, M.L.; Meo, M.G.; Russo, P. Simulation of fire scenarios due to different vehicle types with and without traffic in a bi-directional road tunnel. *Tunn. Undergr. Space Technol.* **2013**, *37*, 22–36. [[CrossRef](#)]
25. Yamamoto, K.; Sawaguchi, Y.; Nishiki, S. Simulation of tunnel fire for evacuation safety assessment. *Safety* **2018**, *4*, 12. [[CrossRef](#)]
26. Khaksari, R.; Harun, Z.; Fielding, L.; Aldridge, J. Numerical simulation of the evacuation process in a tunnel during contraflow traffic operations. *Symmetry* **2021**, *13*, 2392. [[CrossRef](#)]
27. Na, W.; Chen, C. A Study on the Evacuation Spacing of Undersea Tunnels in Different Ventilation Velocity Conditions. *Fire* **2022**, *5*, 48. [[CrossRef](#)]
28. Kawabata, N.; Wang, Q.; Yagi, H.; Kawakita, M. Study of Ventilating Operation during Fire Accident in Road Tunnels with Large Cross Section. In Proceedings of the 4th KSME-JSME Fluid Engineering Conference, Pusan, Republic of Korea, 18–21 October 1998; pp. 53–56.
29. Wang, Q.; Kawabata, N.; Ishikawa, T. Evaluation of critical velocity employed to prevent the backlayering of thermal fume during tunnel fires. In Proceedings of the International Conference on Applied Computational Fluid Dynamics, Beijing, China, 17–20 October 2000; pp. 404–411.
30. Kunikane, Y.; Kawabata, N.; Takekuni, K.; Shimoda, A. Heat release rate in a large cross section tunnel. *Tunn. Manag. Int.* **2003**, *6*, 22–29.
31. Kawabata, N.; Matsuba, S.; Ishikawa, T.; Okubo, K.; Shimoda, A.; Kunikane, Y. Simulation of water spray for fire accident in large cross section tunnel. In Proceedings of the Tunnel Fire—5th International Conference, Marseilles, France, 6–10 October 2004; pp. 69–78.
32. Yokota, M.; Kawabata, N. A study of Chimney Natural Exhaust Effect for Road Tunnel Fire an Evaluation Using the Numerical Simulation of the Real Scale Tunnel. In Proceedings of the 6th International Conference Tunnel Safety and Ventilation—New Developments in Tunnel Safety, Graz, Austria, 23–25 April 2012; pp. 82–89.
33. Seike, M.; Ejiri, Y.; Kawabata, N.; Hasegawa, M. Suggestion of estimation method of smoke generation rate by CFD simulation and fire experiments in full-scale tunnels. *J. Fluid Sci. Technol.* **2014**, *9*, 1–11. [[CrossRef](#)]
34. Kikumoto, T.; Kawabata, N.; Maruyama, D.; Yamada, M. Behavioral characteristics of hot air flow during fire in a small road tunnel for passenger cars (Examination by numerical simulation). *Jpn. Soc. Civ. Eng.* **2007**, *63*, 448–459. (In Japanese)
35. Seike, M.; Kawabata, N.; Hasegawa, M.; Tanaka, H. Heat release rate and thermal fume behavior estimation of fuel cell vehicles in tunnel fires. *Int. J. Hydrog. Energy* **2019**, *44*, 26597–26608. [[CrossRef](#)]
36. Kawabata, N.; Kunikane, Y.; Takekuni, K.; Shimoda, A. Numerical Simulation of Smoke Descent in a Tunnel Fire. *Tunn. Manag. Int.* **2003**, *6*, 45–52.
37. Kim, E.; Woycheese, J.P.; Dembsey, N.A. Fire dynamics simulator (version 4.0) simulation for tunnel fire scenarios with forced, transient, longitudinal ventilation flows. *Fire Technol.* **2008**, *44*, 137–166. [[CrossRef](#)]
38. McGrattan, K.; Hostikka, S.; Floyd, J.; McDermott, R.; Vanella, M. Fire dynamics simulator technical reference guide volume 1: Mathematical model. *NIST Spec. Publ.* **2022**, *1018*, 29. [[CrossRef](#)]
39. Kawabata, N.; Kawai, Y.; Kunikane, Y. Large eddy simulation of hot gas flow in the tunnel fires. *Abstr. Annu. Meet. Jpn. Assoc. Fire Sci. Eng.* **2003**, 202–205. (In Japanese)
40. Brown, G.O. The history of the Darcy-Weisbeck equation for pipe flow resistance. *Environ. Water Resour. Hist.* **2002**, 34–43. [[CrossRef](#)]

41. Blasius, H. *Das Ähnlichkeitsgesetz bei Reibungsvorgängen in Flüssigkeiten, Forschungs-Arbeit des Ingenieur-Wesens 131*; Springer: Berlin/Heidelberg, Germany, 1913. (In German)
42. Jang, H.M.; Chen, F. On the determination of the aerodynamic coefficients of highway tunnels. *J. Wind. Eng. Ind. Aerodyn.* **2002**, *90*, 869–896. [CrossRef]
43. Jürges, W. *Der Wärmeübergang an Einer Ebenen; Wand, Beihefte Zum Gesundheits-Ingenieur, Reihe 1, Arbeiten Aus Dem Heiz Und Luftungsfach, Herausgegeben Von Der Schriftleitung Des Gesundheits Ingenieurs, IV. Versuchsergebnisse; Verlag von R. Oldenbourg: Munchen/Berlin, Germany, 1924; pp. 39–45. (In German)*
44. Król, A.; Król, M. Numerical investigation on fire accident and evacuation in a urban tunnel for different traffic conditions. *Tunn. Undergr. Space Technol.* **2021**, *109*, 103751. [CrossRef]
45. Qu, X.; Meng, Q.; Liu, Z. Estimation of number of fatalities caused by toxic gases due to fire in road tunnels. *Accid. Anal. Prev.* **2013**, *50*, 616–621. [CrossRef] [PubMed]
46. Seike, M.; Kawabata, N.; Hasegawa, M. Quantitative assessment method for road tunnel fire safety: Development of an evacuation simulation method using CFD-derived smoke behavior. *Saf. Sci.* **2017**, *94*, 116–127. [CrossRef]
47. Ejiri, Y.; Kawabata, N. Smoke generation of fire tests of Real scale tunnel. In Proceedings of the Fluids Engineering Conference the Japan Society of Mechanical Engineers, Kanazawa, Japan, 29–30 October 2005; p. 181. (In Japanese).
48. Seike, M.; Kawabata, N.; Hasegawa, M. Experiments of evacuation speed in smoke-filled tunnel. *Tunn. Undergr. Space Technol.* **2016**, *53*, 61–67. [CrossRef]
49. Seike, M.; Kawabata, N.; Hasegawa, M. Evacuation speed in full-scale darkened tunnel filled with smoke. *Fire Saf. J.* **2017**, *91*, 901–907. [CrossRef]
50. Seike, M.; Lu, Y.C.; Kawabata, N.; Hasegawa, M. Emergency evacuation speed distributions in smoke-filled tunnels. *Tunn. Undergr. Space Technol.* **2021**, *112*, 103934. [CrossRef]
51. Caliendo, C.; Genovese, G.; Russo, I. Risk analysis of road tunnels: A computational fluid dynamic model for assessing the effects of natural ventilation. *Appl. Sci.* **2021**, *11*, 32. [CrossRef]
52. Yamada, T.; Akizuki, Y. Visibility and Human Behavior in Fire Smoke. In *SFPE Handbook of Fire Protection Engineering*, 5th ed.; Morgan, J.H., Ed.; Springer: New York, NY, USA, 2016; Volume II, p. 2181.
53. Purser, D.A. Modelling toxic and physical hazard in fire. *Fire Saf. Sci.* **1989**, *2*, 391–400. [CrossRef]
54. Frey, S.; Riklin, N.; Brandt, R.; Heger, O.; Kohl, B. Modelling of Tunnel Ventilation’s Influence on Fire Risk—A Detailed Comparison of Model Assumptions and Their Potential Influence. In Proceedings of the International Symposium Aerodynamics, Ventilation and Fire in Tunnels, Athen, Greece, 25–27 September 2019; pp. 1–15.
55. Yang, D.; Huo, R.; Zhang, X.L.; Zhao, X.Y. Comparison of the distribution of carbon monoxide concentration and temperature rise in channel fires: Reduced-scale experiments. *Appl. Therm. Eng.* **2011**, *31*, 528–536. [CrossRef]
56. National Research Council. *Acute Exposure Guideline Levels for Selected Airborne Chemicals*; The National Academies Press: Washington, WA, USA, 2009; Volume 8, p. 35. Available online: <http://www.nap.edu/catalog/12770.html> (accessed on 5 March 2023).
57. The National Institute for Occupational Safety and Health (NIOSH). Carbon Monoxide Immediately Dangerous to Life or Health ConcentrationS (IDLH), Carbon Monoxide, 2014. Available online: <https://www.cdc.gov/niosh/idlh/630080.html#print> (accessed on 8 November 2022).
58. Chen, L.Y.; Seike, M.; Kawabata, N.; Hasegawa, M.; Chien, S.W.; Shen, T.S. Walking speed probability distribution in smoke-filled tunnel experiments. *J. Chin. Inst. Eng.* **2022**, *45*, 661–668. [CrossRef]
59. Seike, M.; Kawabata, N.; Hasegawa, M. Walking speed under emergency situation in smoke-filled tunnel with obstacles. *Tunn. Undergr. Space Technol. Inc. Trenchless Technol. Res.* **2023**, *133*, 104939. [CrossRef]

**Disclaimer/Publisher’s Note:** The statements, opinions and data contained in all publications are solely those of the individual author(s) and contributor(s) and not of MDPI and/or the editor(s). MDPI and/or the editor(s) disclaim responsibility for any injury to people or property resulting from any ideas, methods, instructions or products referred to in the content.